MCB Accepted Manuscript Posted Online 20 January 2015
Mol. Cell. Biol. doi:10.1128/MCB.01071-14

Muscle-derived ERK1/2 MAP kinases are required for the maintenance of adult myofibers and their neuromuscular junctions

Bonnie Seaberg,[a] Gabrielle Henslee,[a] Shuo Wang, [a] Ximena Paez-Colasante,[a,b,*] Gary E. Landreth[c], Mendell Rimer[a,b,#]

Department of Neuroscience & Experimental Therapeutics, College of Medicine, Texas A&M University Health Science Center, Bryan, Texas USA[a]; Texas A&M University Institute for Neuroscience, College Station, Texas, USA[b]; Department of Neurosciences, Case Western Reserve University School of Medicine, Cleveland, Ohio, USA[c]

Running Head: ERK1/2 in NMJ and myofiber maintenance *in vivo*

#Address correspondence to Mendell Rimer, mjrimer@medicine.tamhsc.edu.

*Present address: Ximena Paez-Colasante, Department of Neurology, University of Michigan, Ann Arbor, Michigan, USA

Word counts: Abstract: 198. Materials and Methods: 1264. Introduction, Results, Discussion (combined): 5888.

ABSTRACT

The Ras-ERK1/2 pathway appears important for the development, maintenance, aging and pathology of mammalian skeletal muscle. Yet no gene targeting of *Erk1/2* in muscle fibers *in vivo* has been reported to date. We combined a germline mutant *Erk1* with Cre-loxP *Erk2* inactivation in skeletal muscle to produce, for the first time, mice lacking ERK1/2 selectively in skeletal myofibers. Animals lacking muscle ERK1/2 displayed stunted postnatal growth, muscle weakness and shorter lifespan. Their examined muscles here, sternomastoid and tibialis anterior, displayed fragmented neuromuscular synapses and a mixture of modest fiber atrophy and loss, but failed to show major changes in fiber type composition or absence of cell surface dystrophin. Whereas lack of only ERK1 had no effects on the phenotypes studied, lack of myofiber ERK2 explained synaptic fragmentation in the sternomastoid, but not the tibialis anterior, and a decrease in the expression of the acetylcholine receptor (AChR) epsilon subunit gene mRNA in both muscles. A reduction in AChR protein was documented in line with the above mRNA results. Evidence of partial denervation was found in the sternomastoid but not the tibialis anterior. Thus, myofiber ERK1/2 are differentially required for the maintenance of myofibers and neuromuscular synapses in adult mice.

INTRODUCTION

Mitogen-activated protein kinases (MAPKs) are components of intracellular signaling modules that control a myriad of cellular processes. MAPK modules consist of 3 core protein kinase components. The most downstream is the actual MAPK, a S/T kinase that phosphorylates the transcription factors, cytoskeletal elements or other kinases, that are the targets of regulation by signaling cascades started at the cell surface. A MAPK is activated by an upstream MAPK kinase (MAP2K), which in turn is activated by a MAP2K kinase (MAP3K). MAP3Ks are usually at the receiving end of signals derived from small, monomeric GTPases such as the Ras family or by other more intricate mechanisms (1). In mammalian cells, the prototypical MAPK module is composed of the MAPKs extracellular-signal regulated kinases 1 and 2 (ERK1/2), the MAP2Ks MEK1/2 and the MAP3K Raf. ERK1/2 regulate normal cellular responses to multiple growth factors and cytokines in proliferation, differentiation and apoptosis (2, 3).

Multiple studies suggest an important role for the Ras-ERK1/2 pathway in the development, normal maintenance, aging and pathology of mammalian skeletal muscle. Thus ERK1/2 activity has both stimulatory and inhibitory roles in the differentiation of cultured skeletal myotubes that vary with the stage of this protracted process (4–8). ERK1/2 have been implicated in the maintenance of adult skeletal muscle mass (9), and, seemingly paradoxically, in the control of both the fast-twitch (10), and the slow-twitch (11) fiber type phenotypes. Alterations in levels of ERK1/2 activity in aging rodent muscle correlate with sarcopenia (12), the loss of muscle mass and strength that occurs with aging (13). Ras-ERK1/2 pathway activity dysregulation underlies the pathology of

neuromuscular diseases such as autosomal Emery-Dreifuss muscular dystrophy (14) and of the RASopathies, a group of rare genetic diseases with accompanying skeletal muscle abnormalities (15–17). Our own work in cultured myotubes (18) suggests a modulatory role for ERK1/2 on the activity of agrin (19), a key synaptogenic factor in the formation and maintenance of the neuromuscular junction (NMJ), the synapse between a motoneuron and a skeletal muscle fiber (20). In vitro and in vivo studies implicated ERK1/2 in the control of synapse-specific expression of acetylcholine receptor (AChR) subunit genes at the NMJ, particularly of *Chrne*, the gene coding the adult AChRε subunit (21–23).

Most of the experiments that have been carried out to characterize the role of ERK1/2 in skeletal muscle biology have been done in cultured cells, using either pharmacological tools, in particular MEK inhibitors, siRNA, constitutively active or dominant-negative constructs for the different components of the Ras-ERK1/2 pathway. However, no gene targeting investigations on the role of ERK1/2 in developing muscle fibers *in vivo* have been reported to date. We combined a germline *Erk1* mutant with Cre-loxP inactivation of *Erk2* in skeletal muscle to produce, for the first time, mice lacking ERK1/2 selectively in skeletal myofibers. We report that ERK1/2 are required for the maintenance of myofibers and NMJs in adult animals.

MATERIALS AND METHODS

Ethics statement. Care and treatments of all animals followed the National Institutes of Health Guide for the Care and Use of Laboratory Animals and were approved by the Institutional Animal Care and Use Committee of Texas A&M University under animal use protocol 2012-168.

Mice and genotyping. The Cre-driver mice in which Cre is under control of the human α-skeletal muscle actin promoter are represented as *Hsa-Cre*$^{+/-}$. The *Erk2* floxed allele is represented as *Erk2*^{f}. Local colonies were established from breeders obtained initially as follows: *Hsa-Cre*$^{+/-}$ mice from Jackson labs (JAX stock# 006149); *Erk1*$^{+/}$; *Erk2*$^{f/+}$ and *Erk2*$^{f/f}$ mice from the Landreth lab, Case Western Reserve University. These crosses were used to generate experimental animals: *Erk1*$^{-/-}$ mice came from *Erk1*$^{+/-}$ X *Erk1*$^{-/-}$. Mice deficient in muscle ERK2 (referred in the text as *mErk2*^{CKO}) came from *Hsa-Cre*$^{+/-}$; *Erk2*$^{f/+}$ X *Hsa-Cre*$^{-/-}$; *Erk2*$^{f/f}$. Mice deficient in germline ERK1 and muscle ERK2 (referred in the text as DKO) came from *Hsa-Cre*$^{+/-}$; *Erk1*$^{+/-}$; *Erk2*$^{f/f}$ X *Hsa-Cre*$^{-/-}$; *Erk1*$^{-/-}$; *Erk2*$^{f/f}$. Genotyping was done by PCR with the following primers: *Cre*: 5'-GCGGTCTGGCAGTAAAAACTATC-3'; 5'-GTGAAACAGCATTGCTGTCACTT-3'. *Erk1*: wild type and null allele were detected with these primers: 5'-GTATCTTGGGTTCCCCATCC-3'; 5'-GGGGAACTTCCTGACTAGGG-3'; 5'-GCTCCATGTCGAAGGTGAAT-3'. *Erk2*: wild type and floxed allele were detected with these primers: 5'- AGCCAACAATCCCAAACCTG-3'; 5'-GGCTGCAACCATCTCACAAT-3'. Mice were housed at 25°C with a 12h light/dark cycle, fed *ad libitum* and monitored daily.

Western blotting. Muscles were dissected, snapped frozen in liquid N_2 and stored at -80°C until use. Most tissue homogenates were prepared in the following buffer: 25mM Tris pH 7.4, 95mM NaCl, 1mM EDTA, 1mM EGTA, 1% SDS, 10% Protease Inhibitor Cocktail (P8340, Sigma), 5mM NaF, 2mM Na_3VO_4, 2.5mM $Na_4P_2O_7$. Lysates used to analyze p38 were made in 1% Triton X-100, 30 mM triethanolamine pH 7.5, 50 mM NaCl, 5 mM EGTA, 5 mM EDTA, with the same phosphatase and protein inhibitors as

above. Total protein was measured using Biorad Protein Assay, and 50 µg per sample were run on 10% acrylamide denaturing gels. Proteins were transferred to polyvinylidene difluoride (PVDF) membranes using a semi-dry blotter (Biorad). Suppliers of primary antibodies and dilutions were: Epitomics: Anti-ERK1 (1171-1, 1:1000); anti-ERK2 (1586-1, 1:1000). Cell Signaling: Anti-tERK1/2 (9102, 1:1000); anti-p38 (9212, 1:1000); anti-pp38 (4511, 1:1000); anti-JNK (9252, 1:500). Santa Cruz Biotechnology: Anti-pERK1/2 (SC7383, 1:200); anti-pJNK (SC6254, 1:200). Sigma: Anti-α-Tub (T6199, 1:4000). Horseradish peroxidase-secondary antibodies (SC2020 and SC2031, Santa Cruz Biotechnology; 111-035-003 and 315-035-003, Jackson Immunoresearch) were used at 1:1000-1:3000. Blots were visualized by chemiluminescense following manufacturer's instructions (PerkinElmer). Images were acquired and analyzed with an AlphaImager gel imaging system (Protein Simple).

AChR affinity isolation and probing. AChRs were isolated and detected as previously described with minor modifications (24). Briefly, muscles were lysed in 1% Triton X-100, 30 mM triethanolamine pH 7.5, 50 mM NaCl, 5 mM EGTA, 5 mM EDTA, 10% Protease Inhibitor Cocktail (P8340, Sigma), 5mM NaF, 2mM Na_3VO_4, 2.5mM $Na_4P_2O_7$,. One mg of total protein per muscle lysate was incubated for 30 min with 200 nM biotin-α-bungarotoxin (BBTX; B-1196, Life Technologies) at 4°C. Streptavidin–agarose (SA100-04, Life Technologies) was used to precipitate the BBTX–AChR complexes. After washing with lysis buffer, complexes were separated by SDS-PAGE, transferred to PVDF membranes, and probed with a goat-polyclonal to AChRε at 1:250 (ab166931, Abcam). Bands were visualized by chemiluminescence and quantified as above.

Grip strength assay. Forelimb grip strength was assessed with a grip strength meter with single sensor and a standard pull bar and software (Columbus Instruments) as previously described (25). Briefly, mouse was directed to grip the bar with forelimbs then pulled off the bar by the tail, and peak force (in g) was recorded for 3 consecutive trials. Trial averages were normalized to body weight (g).

Rotarod. A Rotarod Series 8 (IITC Life Science Inc.) was used for rotarod analysis. From 7-19 weeks of age, mice were subjected to two rotarod modes every other week. First, constant speed of 4 rpm for 5 min, immediately followed by 0.1 rpm/sec acceleration to a maximum speed of 30 rpm, ending the trial at 5 min (25). Time-to-fall (sec) was recorded for both modes. Mice were allowed to rest for 10 min and the above procedure was repeated twice more for a total of 3 trials. Time-to-fall per mode was averaged for the 3 trials. Data for week 7 were considered as adaptation and are not presented in the results.

Whole mount staining, confocal microscopy and NMJ morphological characterization. Whole mount staining of sternomastoid (STN) and tibialis anterior (TA) was essentially done as previously described (26). Anti-synaptophysin (SYN) (180130, Life Technologies) was used at 1:200, fluorescein-BTX (F-1176, Life Technologies) was used at 1:1000. Rhodamine-rabbit secondary antibody (111-025-144, Jackson Immunoresearch) was used at 1:400. At the dilution of anti-SYN used, both nerve terminal and pre-terminal axon were visible in many cases. Vectashield (Vector Laboratories)-mounted muscle bundles from these preparations were imaged on an A1 confocal microscope (Nikon), with 40X (NA 1.30) and 60X (NA 1.40) oil immersion objectives. Images were acquired and maximal intensity projections were generated with

NIS Elements software (Nikon). On the maximal projections, NMJ morphology was studied by counting: (i) number of AChR domains per endplate; (ii) faint or weakly-BTX stained NMJs, defined as those endplates with noticeably weaker or dimmer BTX stain relative to others on the same field; (iii) terminal sprouts, defined as extensions of any length and direction of nerve terminal staining beyond AChR stain at a synaptic site.

Central myonuclei quantification. One slide with several 12-14 µm-thick frozen cross sections from the belly of a STN was stained for H&E by a standard procedure. Images from 5, 20X fields per slide were acquired with an EC3 camera and software (Leica), mounted on an Eclipse E1000 microscope (Nikon). Total number of fibers and fibers with central nuclei were counted. Replicates within a genotype were averaged for final quantification.

Real-time quantitative PCR. Total RNA extraction, reverse transcription, and real-time PCR were done essentially as previously reported (26). 200 ng of total RNA per sample were used to generate cDNA. All Taqman primer sets and probes were from ABI/Life Technologies as follows: *Chrna*, Mm00431629_m1; *Chrnb*, Mm00680412_m1; *Chrnd*, Mm00445545_m1; *Chrne*, Mm00437411_m1; *Chrng*, Mm00437419_m1; *Runx1*, Mm01213404_m1; *Myh3*, Mm01332463_m1; 18S rRNA, 4333760F.

Myofiber morphological analysis. Dystrophin staining of transverse frozen sections was performed essentially as previously described (26), except that sections were not fixed and individual primary antibodies to myosin heavy chains (MyHCs) were co-incubated with the anti-dystrophin antibody (15277, Abcam). All MyHC antibodies were from the Developmental Studies Hybridoma Bank as follows: type 1, A4.840; type 2A, SC-71; type 2B, 10F5; type 2X, 6H1. All but SC-71, which was sometimes used at 1:600, were

used undiluted. Fluorophore-conjugated secondary antibodies that matched the primary isotype (Jackson Immunoresearch and Sigma) were used at 1:400 and 1:128, respectively. Fiber area analysis was carried out as previously described (26) on overlapping 10X images that covered an entire muscle cross section. Care was taken not to measure the same fibers more than once. For fiber typing, 10X overlapping images of individual MyHC type and dystrophin staining were assembled in Photoshop (Adobe) to reconstruct an entire muscle cross section. Total fibers were counted from the dystrophin staining, and MyHC type fibers were counted from the respective antibody staining. Replicates per muscle/genotype were averaged for final quantification.

Statistical analysis. Quantitative data are expressed as mean ± SEM. Kaplan-Meier survival curves were generated and tested for statistical significance using the log-rank test with Prism5 (GraphPad Software). Analysis of the Variance (ANOVA) was performed at http://vassarstats.net/. One- and two-sample Student's t-tests were computed with Prism5 (GraphPad Software) and Microsoft Excel (Microsoft Corporation), respectively. Wilcoxon Rank Sum test probabilities were computed at http://socr.stat.ucla.edu. Significance was set at $p < 0.05$.

RESULTS

Generation of skeletal muscle-selective *Erk2* conditional mice and of mice lacking ERK1/2 in skeletal muscle fibers.

While germline *Erk1*$^{-/-}$ mice are viable and fertile but display defective thymocyte maturation (27, 28), *Erk2*$^{-/-}$ mice are early embryonic lethal due to failure to form the ectoplacental cone and extra-embryonic ectoderm (29, 30). *Erk2*$^{-/-}$ embryos do not form mesoderm (31). A conditional *Erk2* allele (*Erk2*$^{f/f}$) was generated by Landreth and

colleagues (32). To delete *Erk2* selectively in developing and adult skeletal muscle fibers, *Erk2*$^{f/f}$ mice were crossed to mice that express Cre under control of the human α-skeletal muscle actin promoter (*Hsa-Cre*$^{+/-}$) (33, 34). Expression of Cre under this promoter was detected beginning at embryonic day (E) 9.5 onwards (33) and in skeletal muscle is restricted to myofibers. Neither myoblasts nor satellite cells express Cre in these mice (35). *Hsa-Cre*$^{+/-}$*; Erk2*$^{f/f}$ mice (hereafter referred to as *mErk2*^{CKO}) were viable and fertile. Western blots of muscle extracts showed a ~90% reduction in ERK2 levels in *mErk2*^{CKO} mice (Fig 1A). Full removal of ERK2 from whole muscle tissue was not expected as myofiber nuclei only represent ~41% of the total nuclei in muscle tissue (36). ERK1 levels in *mErk2*^{CKO} mutants were ~20% lower than in controls (Fig 1B). As expected, ERK1 was completely absent in muscle homogenates from germline *Erk1*$^{-/-}$ mice (Fig 1C, top panel). Mice lacking both ERK1 and ERK2 in skeletal muscle fibers were generated by crossing *Erk1*$^{-/-}$ and *mErk2*^{CKO} animals (for details see methods). Skeletal muscle from *Hsa-Cre*$^{+/-}$*; Erk1*$^{-/-}$*; Erk2*$^{f/f}$ mice (hereafter referred to as DKO) lacked ERK1 and had a great reduction of ERK2 as expected (Fig 1C, top panel). Phosphorylated ERK2 (pERK2) was diminished to similar extent in both *mErk2*^{CKO} and DKO mutants, in direct correspondence to the decrease in total ERK2 (Fig 1C, bottom panel). The reduction in ERK2 was specific to skeletal muscle as it was not observed in heart, spinal cord or liver (Fig 1D). However, a ~50% reduction in kidney ERK2 levels was detected in DKO animals relative to control (Fig 1D).

Mice lacking ERK1/2 in skeletal muscle fibers are viable but display stunted postnatal growth, muscle weakness and shorter lifespan.

228 DKO animals were born at the expected Mendelian ratios predicted from the
229 crosses. Thus, from the cross *Hsa-Cre*$^{-/-}$; *Erk1*$^{-/-}$; *Erk2*$^{f/f}$ x *Hsa-Cre*$^{+/-}$; *Erk1*$^{+/-}$; *Erk2*$^{f/f}$,
230 78/317 pups (i.e. the expected ¼) showed the *Hsa-Cre*$^{+/-}$; *Erk1*$^{-/-}$; *Erk2*$^{f/f}$ genotype when
231 assayed post-weaning. We followed their weight starting at week 4 after birth. Starting at
232 week 7, we also assayed muscle strength and overall motor coordination and fatigue
233 resistance by measuring forelimb grip strength and by subjecting mice to a rotarod
234 protocol, respectively. Muscle ERK2-deficient, and germline ERK1-deficient mice
235 showed no difference in weight progression and forelimb grip strength relative to control
236 animals (*Hsa-Cre*$^{-/-}$; *Erk1*$^{+/+}$; *Erk2*$^{f/f}$), whereas DKO mutants failed to gain weight and
237 showed a progressive loss of grip strength as young adults (Fig 2A and B). Interestingly,
238 double mutants could be divided into two groups according to how fast they lost weight
239 (Fig 2A). "Severe" animals lost weight rapidly starting at about 7 weeks of age, while
240 "mild" double mutants were able to keep their weight at that age but clearly failed to keep
241 up with controls or single mutants (Fig 2A). We currently do not understand the basis of
242 this differential effect on weight. When normalized to body weight, both types of DKO
243 mutants showed very similar reduction of grip strength (Fig 2B). "Severe" mice were not
244 tested with the rotarod due to their overall frailty. However, "mild" DKO mice displayed
245 a clear tendency to fall earlier from an accelerating rotarod (Fig 2C). DKO mutants do
246 not survive as long as controls or single mutants. Their deaths were either sudden and
247 unexplained or followed weight loss of such severity that demanded humane euthanasia
248 according to protocol guidelines. Their median lifespans were: 71 days, n=23 (severe);
249 121 days, n=7 (mild). (Fig 2D). Interestingly, all 5 registered deaths among the "mild"
250 DKO animals were males, while the 2 females remained alive. Kyphosis, a sign of

251 muscle weakness, was clearly evident in the long-surviving animals (Fig 2E) and in at
252 least one of the males that lived for 120 days. Thus, these results suggest that muscle
253 depletion of either ERK1 or ERK2 has no overt phenotypic effects on the mice and that
254 ERK1 and ERK2 together are required for myofiber postnatal maintenance or growth.

255 **Extensive fragmentation of the mature NMJ in ERK1/2-deficient muscle.**

256 These studies were prompted by our previous results with cultured myotubes. We
257 found that agrin stimulated the transient activation of ERK1/2 in an LDL receptor related
258 protein 4 (Lrp4)/muscle-specific kinase (MuSK)-dependent fashion. Pharmacological
259 blockade of this activation failed to inhibit agrin-induced acetylcholine receptor (AChR)
260 clustering. Instead, it potentiated it by ~60%. These, and other observations, led us to
261 propose that agrin-induced ERK1/2 activation is part of a feedback loop that keeps
262 agrin's clustering activity in check, at least *in vitro* (18). The fact that the DKO mice are
263 viable and appear normal well after NMJs have formed and matured suggests that this
264 ERK-dependent feedback mechanism is dispensable for the formation of the NMJ in
265 vivo. However, it was still possible that ERK signaling had some role in NMJ
266 maintenance, especially in light of the overall postnatal muscle weakness of the DKO
267 mice (Fig 2). We stained whole mounts of the neck sternomastoid (STN) muscle in
268 control and DKO young adults for pre- and postsynaptic markers and examined the
269 samples under confocal microscopy. The STN has been used by others to study the
270 effects of aging and amyotrophic lateral sclerosis (ALS) on the structure of the mature
271 NMJ (37–39). In control muscle, the NMJs exhibited their characteristic "pretzel" shape
272 with long, continuous domains of postsynaptic AChRs labeled by α-bungarotoxin (BTX)
273 tightly apposed by nerve terminals labeled by synaptophysin (SYN) (Fig 3A). In STN

DKO muscles, many NMJs looked very fragmented with small, mostly round AChR domains variably apposed to nerve terminal staining (Fig 3B,C). This synaptic fragmentation, reminiscent of NMJs in aged normal animals (37, 38, 40), mdx and utrophin/dystrophin knockout mice (41, 42), was observed in males and females from both "severe" and "mild" DKO muscle (Fig 3B,C).

Lack of myofiber ERK2 is sufficient to observe extensive synaptic fragmentation in the sternomastoid muscle.

Next we sought to explore whether synaptic fragmentation required the deficiency of both muscle ERK1 and ERK2, or whether the lack of only one of these two kinases was sufficient for this phenotype. STNs from control (*Hsa-Cre*$^{-/-}$; *Erk1*$^{+/+}$; *Erk2*$^{f/f}$), *Erk1*$^{-/-}$, *mERK2*^{CKO} and "mild" DKO young adults were dissected, stained and imaged by confocal microscopy as above. We chose to work with the "mild" DKO animals because they survive longer and displayed an overall better health than the "severe" DKO mice. The number of AChR domains per endplate was quantified on NMJs viewed "en face". For animals between 3 to 6 months of age, the average number of AChR domains per endplate was 7.26 ± 0.38 for control (n=85 NMJs, 5 mice), 12.15 ± 1.69 for DKO (n=52 NMJs, 3 mice), 8.38 ± 0.94 for *Erk1*$^{-/-}$ (n=80 NMJs, 4 mice) and 12.93 ± 0.91 for *mErk2*^{CKO} (n=90 NMJs, 6 mice). Thus, endplates from DKO and *mErk2*^{CKO}, but not *Erk1*$^{-/-}$ STN had significantly more AChR fragments on average than control. We plotted the percentage of NMJs vs. the number of AChR domains (in bins of 5) for each genotype (Fig 4A). While a shift to NMJs with larger number of AChR fragments could be appreciated for all 3 mutants, the most striking observation was that NMJs with more than 20 AChR domains were only found in DKO and *mErk2*^{CKO} STN, not in control or

Erk1$^{-/-}$ muscle (Fig 4A). These highly fragmented endplates constituted up to 20% of total NMJs in the *mErk2*^{CKO} STN (Fig 4A). Statistical comparison of the mutant distributions relative to control using the Wilcoxon Rank Sum test showed that only the DKO and *mErk2*^{CKO} distributions were significantly different than control (DKO vs. control: p=0.000003; *mErk2*^{CKO} vs. control: p=0.000002; *Erk1*$^{-/-}$ vs. control: p=0.05). Furthermore, statistical comparison using the same test of the DKO vs. the *mErk2*^{CKO} distributions showed no difference between them (p=0.88). Lastly, as an additional control we quantified AChR domains/NMJ in STN from *Hsa-Cre*$^{+/-}$ driver mice. We found an average of 5.96 ± 0.57 (n=77 NMJs, 2 mice), slightly lower than our control. An example of a highly fragmented synapse in *mERK2*^{CKO} STN is shown in Fig 5A. Therefore, lack of muscle ERK2 is sufficient to yield extensive synaptic fragmentation in the STN.

Differential sensitivity to the lack of ERK2 between different muscles.

Next we studied synapse morphology in the hind limb tibialis anterior (TA) muscle, which was also used recently to study effects of aging on the NMJ (40, 43). The TA showed a different response than the STN (Fig 4B). First, control NMJs were much less fragmented in the TA than the STN to begin with. Average AChR domains per endplate in control TA were 3.85 ± 0.25 (n=65, 4 mice). Second, NMJs in *mErk2*^{CKO} and *Erk1*$^{-/-}$ TA muscles appeared on average as fragmented as control. The former had a mean of 4.30 ± 0.25 AChR domains/endplate (n=112 NMJs, 5 mice), and the latter had 4.91 ± 0.52 (n=32 NMJs, 2 mice). Third, only DKO endplates displayed statistically significant fragmentation as their average number of AChR domains/endplate rose to 6.46 ± 0.75 (n=37 NMJs, 3 mice; p=0.003, Wilconox Sum Rank test). Fourth, NMJs with more than

15 AChR domains were never seen in control or *Erk1*$^{-/-}$ muscle, were extremely rare in *mERK2*^{CKO} TA and reached less than 10% of the junctions in DKO muscle. Fifth, NMJs with more than 20 AChR fragments, which were easily detected in *mErk2*^{CKO} and DKO STN, were absent from the sampled TA junctions, at these ages or even at 9-months of age (data not shown). An example of a control and a highly fragmented NMJ in DKO TA are shown in Figure 5B & C, respectively. Thus at the ages studied, the NMJs of STN and TA displayed differential intrinsic fragmentation and a differential sensitivity to the lack of myofiber ERK1/2.

In order to account for the inherent differences in fragmentation of control NMJs between STN and TA that our data reveal (Fig 4), we propose that a fragmented NMJ could be defined as one having more AChR domains than the control median. The median number of AChR domains were 7 and 3, for control NMJs in STN and TA, respectively. Using this criterion, synaptic fragmentation becomes a predominant feature in the majority of NMJs from DKO muscle as ~70% of the sampled NMJs had more AChR domains than their respective control medians. Thus, 71.15% (37/52) and 67.57% (25/37) NMJs in DKO STN and TA showed more than 7 and 3 AChR domains, respectively. This high-level of fragmentation above control median was also reached in the *mErk2*^{CKO} STN (66.67%; 60/90).

Absence of central myonuclei in muscle ERK2-deficient sternomastoid

Others have suggested that synaptic fragmentation in aging and dystrophic muscle is due to degeneration/regeneration cycles in the synaptic portion of the muscle fiber (38, 41). We sought to determine if the same was happening in *mErk2*^{CKO} and DKO muscle. Nuclei within normal muscle fibers localize towards the periphery of the cell, adjacent to

the sarcolemma. Muscle fiber damage induces degeneration of the old fibers and regeneration of new ones, which are derived from satellite cells, muscle stem cells present in the tissue (44). A hallmark of this process is the accumulation of myonuclei towards the center of the cell. We counted fibers with central nuclei in transverse sections of STN stained for hematoxylin & eosin (H&E). Numbers of myofibers with central nuclei in control, *Erk1*$^{-/-}$ and *mErk2*^{CKO} STN did not differ from each other, hovering around 2% (Fig 6). DKO STN had more fibers with central nuclei than control, but they only reached about 4% of the total (Fig 6). Experiments with Evans blue dye confirmed sarcolemma integrity in *mErk2*^{CKO} muscle (data not shown). Thus NMJ fragmentation was prominent in the *mErk2*^{CKO} STN despite it having the same percentage of fibers with central nuclei as control. Moreover, a doubling in the number of fibers with central nuclei in the DKO STN did not enhance NMJ fragmentation quantitatively (Fig 4A).

ERK1/2 regulate AChR levels at the NMJ.

In addition to the synaptic fragmentation studied above, we observed that about a third of NMJs in DKO muscles had relatively weak or sometimes faint BTX staining even in the presence of strong nerve terminal staining (Fig 7A). Quantification showed that only ~6% of control NMJs, but ~29% and ~38% of endplates in DKO STN and TA respectively, showed dim AChR stain (Fig 7B). While the fraction of endplates from *Erk1*$^{-/-}$ muscle with dim AChR staining was similar to control, it tended to be higher in *mErk2*^{CKO} muscles, but only reached statistical significance in DKO samples (Fig 7B; p=0.03 STN; p=0.006 TA). To check if this apparent reduction in surface AChR protein levels was accompanied by a decrease in mRNA levels of its encoding subunit genes, we used real-time PCR to measure steady state levels for the four genes that encode the adult

Molecular and Cellular Biology

366 AChR (45). Cycle threshold (Ct) values obtained for 18S rRNA were used to equalize
367 differences in total RNA per sample (26). Transcript level fold-change was determined
368 by the $2^{-DeltaDeltaCt}$ method (46) and values were normalized to the Ct values obtained for
369 control muscle for each gene (Fig 7C). We found that *Chrne* mRNA was consistently
370 reduced almost 2-fold in both $mErk2^{CKO}$ and DKO muscle. The reduction was
371 statistically significant in DKO TA and $mErk2^{CKO}$ STN and TA, but was borderline
372 (p=0.05) in the DKO STN (Fig 7C). *Chrnd* mRNA levels were essentially similar to
373 control regardless of genotype or muscle examined (Fig 7C). *Chrna* and *Chrnb* mRNAs
374 tended to be slightly lower than control in $mErk2^{CKO}$ and DKO TA, while they tended to
375 increase particularly in the DKO STN (Fig 7C). Lack of only ERK1 did not affect the
376 mRNA levels for the subunits of the adult receptor (Fig 7C), nor was *Chrne* mRNA
377 different between control and $Hsa\text{-}Cre^{+/-}$ driver muscle (data not shown). Thus, a
378 somewhat selective, muscle-ERK2-dependent reduction in mRNA *Chrne* expression was
379 observed. We next checked if the expression of AChRε protein was also affected in DKO
380 mice. We affinity-purified AChRs from lysates of control and DKO TA muscle using
381 biotinylated BTX and streptavidin-agarose and probed for AChRε subunit by Western
382 blotting. In the DKO TA there was as highly-statistically significant decrease in *Chrne*
383 mRNA (Fig 7C). AChRε protein in DKO TA was ~2-3-fold lower than in control
384 (p=0.03, Fig 8). *Chrne*, the gene encoding the AChRε subunit indicative of the adult
385 receptor is transcribed almost exclusively at the synaptic site (47), so its transcription
386 reflects the production of the synaptic AChR protein. Taken together, the weaker AChR
387 staining at about a third of DKO NMJs, the decrease in AChRε protein demonstrated in

the DKO TA, and the reduction in *Chrne* mRNA levels in *mErk2*^{CKO} and DKO muscle suggest that ERK1/2 regulate expression of the synaptic AChR.

Most prominently in DKO STN, we observed NMJs with AChR patches without overlying SYN staining (i.e. aneural AChR patches, Fig 3) and evidence of nerve terminal sprouting (as illustrated in Fig 7A, top panel). Thus, 45% NMJs (18/40, 3 mice) in the DKO STN, while 16% in control STN (6/38, 4 mice) had terminal sprouts. Because these morphological features are hallmarks of partial denervation (48), we next used real-time PCR to check for mRNA levels for *Chrng*, the gene encoding the distinctive AChRγ subunit of the fetal AChR (45), which is strongly induced by functional denervation in the adult (49). *Chrng* mRNA levels were similar to control in TA muscle from all three mutant genotypes. However, *Chrng* mRNA was moderately increased in *mErk2*^{CKO} STN (2-fold) and reached 40-fold induction in the DKO STN (Fig 7D). mRNA for *Runx1* and the embryonic myosin heavy chain *Myh3*, two other genes strongly induced by denervation (50), were also selectively increased in DKO STN (Fig 7E). The sharp increases in these denervation markers in the DKO STN, but not the DKO TA, were consistent with the trend towards elevated mRNA levels for *Chrna*, *Chrnb* and *Chrnd* in the DKO STN, but not in the DKO TA (Fig 7C), as these AChR genes are also induced by denervation (51).Thus, together these results suggest that loss of myofiber ERK1/2 led to significant partial denervation selectively in the STN.

Myofiber number, size and type effects.

Lastly, we studied myofiber number, size and type in STN and TA muscles to determine whether there was a correlation between potential changes in these parameters and the synapse maintenance phenotypes described above. Cross sections from the belly

Molecular and Cellular Biology

411 of the muscles were co-stained for dystrophin, to mark the boundaries of individual
412 myofibers, and for the 4 canonical myosin heavy chain (MyHC) isoforms that define
413 adult fiber types (1, 2A, 2B, 2X) (52). Dystrophin was present on the surface of muscle
414 fibers of these DKO muscles just as it was in controls and single *Erk* mutants (Fig 9
415 A,B). Total number of fibers per TA cross section were similar across all four genotypes,
416 while there was a statistically significant 21% reduction in fiber numbers limited to the
417 DKO STN (p=0.02, Fig 9C). DKO STN and TA showed modest average fiber atrophy
418 (~14% and ~11%, respectively) that was statistically significant for the DKO TA
419 (p=0.008, Fig 9D). The $Erk1^{-/-}$ and $mErk2^{CKO}$ muscles tended to have slightly
420 hypertrophied fibers on average compared to controls (Fig 9D). Thus, the modest fiber
421 atrophy in both TA and STN together with the fiber loss in the STN, are consistent with
422 the lower weight of DKO animals relative to controls (Fig 2A). We sought to determine
423 the fiber type composition of the STN and TA in our *Erk1/2* mutant mice. In the adult
424 mouse, STN and TA are predominantly fast-fiber muscles (53–55). Our experiments
425 confirmed these published observations as our control and 3 mutant STN and TA muscles
426 had a maximum of 0.2% type 1 fibers (data not shown). Analysis of MyHC staining in
427 STN showed ERK1-lacking mice were similar to controls in the distribution of fast fibers
428 (2A, 2B, 2X) (Fig 9E). There was a tendency towards fewer 2B and more 2A fibers than
429 control in DKO STN that did not reach statistical significance (Fig 9E). $mErk2^{CKO}$ and
430 DKO STN displayed a statistically significant ~7% increase in 2X fibers (p=0.004 and
431 p=0.03, respectively, Fig 9E). Although the variability in the data prevents a clear-cut
432 conclusion, this slight increase in 2X fibers seems to be at the expense of 2B fibers.
433 Mutant TA was no different to control regarding fast fibers (Fig 9F). Thus the analysis of

Molecular and Cellular Biology

the predominantly fast-twitch muscles STN and TA showed only modest changes in fiber type composition due to lack of muscle ERK1/2. Consistent with this conclusion, and with its proposed role in regulating fiber type composition (56), levels of active p38 MAPK were unaltered in DKO muscle relative to control (Fig 10). Active c-jun NH_2-terminal kinase (JNK) levels in DKO were also statistically similar to control. Fold change vs. control: STN p46JNK: 0.99±0.10; STN p54JNK: 0.52±0.05; TA p46JNK: 1.79±0.76; TA p54JNK: 0.55±0.19.

DISCUSSION

We have for the first time selectively abrogated ERK1/2 in skeletal muscle fibers. We found that ERK1/2 are needed for the maintenance of myofibers and NMJs. DKO animals displayed stunted postnatal growth, muscle weakness and shorter lifespan. The muscles examined here, STN and TA, displayed a combination of modest fiber atrophy and loss without major changes in fiber type composition or absence of cell surface dystrophin. Loss of myofiber ERK1/2 yielded both overlapping and distinct changes in synaptic morphology and AChR gene expression that depended on the muscle studied. Whereas lack of only ERK1 had no apparent effects on the phenotypes studied, lack of myofiber ERK2 explained synaptic fragmentation in the STN, but not the TA, and a decrease in the expression of *Chnre* mRNA in both muscles. A corresponding reduction in AChR protein was documented in the TA. Evidence of partial denervation was also found in the STN but not the TA. Thus, myofiber ERK1/2 are differentially required for the maintenance of myofibers and neuromuscular synapses in adult mice.

The cause/effect relationship between muscle weakness and stunted growth in the DKO mice is unclear. One possibility is that muscles involved in mastication and

457 swallowing become weak leading to reduced food intake and weight loss. Although the
458 weight loss of the DKO mice correlated with the combined muscle fiber loss and atrophy
459 observed in their STN and TA muscles, it is possible minor renal problems might have
460 also contributed to this phenotype. Kidneys from DKO mice had about half ERK2 levels
461 than control (Fig 1D). However, only a few isolated single cells in adult kidney tissue
462 express a LacZ reporter that is driven by the same Hsa-Cre mice used here
463 (http://www.informatics.jax.org/recombinase/specificity?id=MGI:2447635&systemKey=
464 4856358). It is unlikely that this low level of expression accounts for the 50% reduction
465 in kidney ERK2 in DKO mice. This reduction, and perhaps any ensuing renal
466 complications, may be secondary effects stemming from the overall muscle weakness.
467 We do not know why the DKO mice die. All of the DKO mild animals that die were
468 males while the surviving ones were females. One of the male DKO mild animals that
469 died at 16 weeks of age displayed kyphosis and showed compromised respiration before
470 humane euthanasia**.** However, other animals died younger and failed to exhibit
471 respiratory distress or kyphosis that was evident to the naked eye. Moreover, the
472 surviving DKO mild females show clear kyphosis (Fig 2E). Future experiments will be
473 needed to clarify these issues.
474 There was an intrinsic difference in fragmented NMJs between control STN and
475 TA muscles. The average NMJ in control STN had about twice the number of AChR
476 domains than the average NMJ in control TA. This correlated with the sensitivity to NMJ
477 fragmentation in these muscles following the reduction in ERK1/2. Even after abrogation
478 of myofiber ERK1/2, this difference was maintained as the most fragmented synapses
479 occurred in the STN and not the TA. It remains possible that these differences disappear

480 in older animals. Wild type TA and STN muscles showed no difference in NMJ
481 fragmentation when examined at 2 years of age (39). However, synaptic fragmentation in
482 that study was defined differently than here. To account for the intrinsic differences in
483 fragmentation of control NMJs in various muscles, we propose that a fragmented NMJ
484 could be defined as one having more AChR domains than the control median. In control
485 muscle, the frequency of fragmented synapses using this criterion will always be by
486 definition 50% at most. Two other groups previously used a threshold of AChR
487 fragments to define a fragmented NMJ. Valdez and colleagues (39, 40), defined a
488 fragmented NMJ as one having 5 or more AChR islands or a segment of the postsynaptic
489 apparatus with severe abnormalities such as a small or irregularly shaped AChR cluster.
490 Li and co-workers (38) defined a fragmented NMJ as one having 10 or more AChR
491 domains. When applied to our data, the Valdez criterion suggests the puzzling conclusion
492 that most of the NMJs in control STN are fragmented. In this regard, our control
493 genotype was not wild type for *Erk2*; it was $Erk2^{f/f}$. Because the average AChR
494 patches/NMJ in the STN from the Cre driver mice (genotype $Erk1^{+/+}$; $Erk2^{+/+}$) was a bit
495 lower than in our control STN, it is possible that the $Erk2^{f}$ allele might have a small effect
496 on fragmentation. Li and colleagues studied the STN and their more stringent criterion
497 perhaps resulted from studying this muscle, whose synapses appear particularly prone to
498 fragmentation. This criterion was rather uninformative for our experiments in the TA
499 because it sets the threshold for fragmentation (≥10 fragments) even above the average
500 AChR domains per NMJ obtained in the DKO TA (~6.46). Thus we believe our control-
501 median-based criterion, in combination with the statistical analysis in Figure 4, is more

502 fitting to define a fragmented NMJ and to account for the intrinsic differences in
503 fragmentation that may occur among synapses in various muscles.

504 Unlike in the TA, loss of myofiber ERK2 in the STN was sufficient to yield the
505 same levels of synaptic fragmentation as in the DKO (Fig 4). These results were
506 unexplained by higher HSA-Cre-driven ERK2 reduction, or higher ERK1 decrease as a
507 consequence of *Erk2*$^{f/f}$ recombination in STN than TA (Fig 1). Nor were endogenous
508 levels of ERK2 higher in control TA than in control STN by Western blotting (data not
509 shown). Although ERK1 and ERK2 are generally viewed as functionally redundant, the
510 differential embryonic lethality between their germline mutants and other evidence (57–
511 59), suggest specific roles for these two kinases in some physiological contexts.
512 Alternatively, the more dramatic phenotypes we find in *mErk2*^{CKO} animals may simply
513 reflect the higher levels of expression of ERK2 relative to ERK1 in skeletal muscle fibers
514 in general.

515 The extensive synaptic fragmentation in the *mErk2*^{CKO} STN failed to correlate to
516 changes in animal weight, forelimb grip strength, survival, fiber number or fiber size,
517 because none of these parameters were different to control. We measured a small increase
518 (~7%) in 2X fibers in the *mErk2*^{CKO} STN relative to control. However, it is unlikely that
519 this accounts for the synaptic fragmentation in this muscle because 67% of the NMJs in
520 the *mErk2*^{CKO} STN were fragmented according to our control-median-based criterion.
521 Although other general changes in the fibers might be linked to synaptic fragmentation,
522 notably changes in metabolic capacity and generation of reactive oxygen species (ROS)
523 (60), our results suggest that ERK2 regulates mechanisms that locally control synapse
524 maintenance. In this context, NMJ fragmentation by excess ROS needs them produced in

525 motoneurons and not in muscle fibers (61, 62). Hence mechanisms underlying NMJ
526 fragmentation by excess ROS and by muscle ERK1/2 deficiency may be fundamentally
527 distinct. There was no correlation between the accumulation of central myonuclei (Fig 6)
528 and the synaptic fragmentation phenotype in *mErk2*^{CKO} and DKO STN (Fig 4A).
529 Postsynaptic mechanisms other than local fiber degeneration/regeneration may account
530 for NMJ fragmentation (63). This does not exclude that some of the fragmented NMJs in
531 our mutant muscles result from degeneration/regeneration in the subsynaptic area. Our
532 measurements of central nuclei were from extrasynaptic regions of the fibers. The
533 relatively small subsynaptic portion of the muscle fiber in mutant muscle could be more
534 prone to damage than the rest of the fiber and/or central nuclei could be transient and
535 migrate quickly to the periphery of the fiber so that we would miss them in our
536 experiments (38).

537 NMJs with dimly BTX-stained AChRs were present both in DKO STN and TA,
538 although they were more easily detected in the latter (Fig 7). Fewer AChRs at the
539 synaptic site could be due to one or a combination of the following processes: Lower rate
540 of synthesis and/or multimeric assembly, higher rate of degradation, lower insertion rate
541 of the receptors in the synaptic sarcolemma or higher retrieval from it. Synthesis depends
542 highly on the rate of local transcription. We found a consistent reduction of the AChRε
543 subunit gene mRNA, which was myofiber ERK2-dependent (Fig 7C). We also
544 documented a corresponding reduction in AChRε protein in the DKO TA (Fig 8).
545 Transcription of all AChR subunit genes is highly enriched at the subsynaptic myonuclei
546 (64–66); however, *Chrne's* is perhaps the most synaptic of them all (47). Thus, a
547 reduction in *Chrne* mRNA is expected to affect the synaptic AChR selectively. This

548 reduction was not due to general fiber atrophy as it was detected in *mErk2*^{CKO} muscle,
549 which was no different to control regarding fiber morphology (Fig 9). The ~2-fold
550 reduction in whole *mErk2*^{CKO} and DKO muscle *Chrne* mRNA may underestimate the
551 reduction at those NMJs with faint AChR staining (Fig 7B). Dominant-negative mutants
552 for Ras, Raf and MEK1 selectively inhibited synapse-specific expression of *Chrne*-
553 luciferase reporters that were expressed in adult TA muscle following DNA injection
554 (23). These experiments suggested that ERK signaling regulates *Chrne* expression at the
555 transcriptional level. Our data showing parallel reductions in both AChRε protein and
556 mRNA are consistent with this mechanism for the role of ERK in controlling *Chrne*
557 expression.

558 The presence of terminal sprouts and of AChR patches lacking apposing nerve
559 terminal staining in some NMJs from DKO STN is consistent with the significant
560 increase in *Chrng* mRNA and suggests that a relevant proportion of NMJs in this muscle
561 are at least functionally denervated. This effect explains the tendency towards increased
562 levels of *Chrna*, *Chrnb* and *Chrnd* mRNA in the DKO STN (Fig 7C), as denervation is
563 well known to induce expression of these AChR subunit genes along the entire muscle
564 fiber (51). It might also explain why *Chrne* mRNA levels in the DKO STN were just
565 borderline different than control ($p=0.05$), while those in *mErk2*^{CKO} STN were
566 significantly lower ($p<0.05$, Fig 8C). This was not observed in the DKO TA, which
567 highlights another important distinction in the response to the lack of myofiber ERK1/2
568 between these two muscles. Unlike synaptic fragmentation in the STN, full expression of
569 this partial denervation-like effect required removal of both ERK1 and ERK2. This
570 suggests that synaptic fragmentation and the apparent denervation are not tightly

571 correlated. The fiber loss and the increased proportion of regenerating fibers detected in
572 the DKO STN (Figs 9 & 6) could account, at least in part, for the upregulation of *Chrng*
573 in this muscle, as increased AChR expression was observed in regenerating muscle (67).
574 In this context, complete denervation is rare in NMJs from aged normal STN, however,
575 partial denervation, terminal sprouts and aneural AChRs were detected (38, 39). Changes
576 in *Chrng* in aged normal STN have not been studied, however, increases in expression of
577 *Chrng* and other denervation markers were reported in aged normal quadriceps (68), and
578 seemed unaccompanied by motoneuron loss (69).

579 The significant fiber loss that we observed in the DKO STN, together with the
580 mild fiber atrophy in DKO STN and TA, are consistent with a role for ERK1/2 in
581 maintaining skeletal muscle mass, and with prior studies that suggested so in C2C12 cells
582 and rats (9). On the other hand, our analysis of fiber type composition in the STN and TA
583 disagrees with the notion that ERK1/2 are essential to preserve the fast-twitch fiber
584 phenotype as previously proposed (10). To inactivate ERK1/2 signaling in vivo, the latter
585 study used overexpression of MAPK phosphatase -1 (MKP-1) by electroporation of adult
586 mouse muscle. However, MKP-1 not only inactivates ERK1/2 but actually shows
587 substrate preference for other MAPKs such as JNK and p38 (56). Thus, the in vivo
588 effects on fast fiber expression reported in this study could have been unspecific to the
589 inactivation of pERK1/2. Others have posited that ERK1/2 are critical to promote slow-
590 fiber differentiation (11). Because the STN and TA muscles studied here bear such a low
591 fraction of type 1 fibers, compelling conclusions about the role of ERK1/2 on the slow
592 fiber phenotype from our animals will have to wait until we examine muscles with
593 significant content of type 1 fibers such as the soleus.

Intrinsic distinctions in the normal development and maintenance of NMJs among different muscles were described (70), and might underlie the differences in the response of the NMJs in STN and TA to the lack of myofiber ERK1/2. Thus, the STN is a delay synapsing muscle while the TA is a fast synapsing one (70). Muscles display differential susceptibility to sarcopenia and to neuromuscular diseases. Some are highly affected while others appear resistant. In many cases, these muscle-selective effects include how their NMJs react to these conditions (39, 71, 72). The mechanisms underlying these unique sensitivities remain elusive and are likely to be complex and condition-specific. Reduction in active ERK1/2 levels with aging were reported in specific muscles of the rat (13). Significant skeletal muscle abnormalities (16, 17) were found in patients suffering from a group of genetic conditions collectively known as RASopathies, in which different components of the Ras/MAPK pathway are anomalously activated (15). Recently, patients with deletions encompassing *MEK2* were shown to have overlapping features with RASopathies, which suggests that haploinsufficiency of Ras-Erk1/2 pathway components is a potential novel mechanism underlying these disorders (73). Our results showing that myofiber-derived ERK1/2 are necessary for the maintenance/growth of adult muscle fibers and for the stability of their NMJs in a muscle-specific fashion further support an important role for this signaling pathway in muscle-selective sarcopenia and are informative as to relevant neuromuscular phenotypes that may be affected by the dysregulation of Ras-ERK signaling in RASopathies.

ACKNOWLEDGENTS

This work was supported by Public Health Service grant NS077177 from the National Institute of Neurological Disorders and Stroke.

617 We thank J. Samuel for access to the confocal microscope, R. Miranda for access
618 to the real-time PCR machine, S. Balaraman for help with qRT-PCR experiments, R.
619 Hastings for making us aware of the AChRε antibody ultimately used here, and W.
620 Thompson for critically reading the manuscript. The MyHC monoclonal antibodies
621 developed by H. Blau, C. Lucas and S. Schiaffino were obtained from the Developmental
622 Studies Hybridoma Bank developed under the auspices of the NICHD and maintained by
623 The University of Iowa, Department of Biology, Iowa City, IA 52242.
624

REFERENCES

1. **Yoon S, Seger R**. 2006. The extracellular signal-regulated kinase: multiple substrates regulate diverse cellular functions. Growth Factors, 2006/01/06 ed. **24**:21–44.
2. **Osborne JK, Zaganjor E, Cobb MH**. 2012. Signal control through Raf: in sickness and in health. Cell Res. **22**:14–22.
3. **Rimer M**. 2011. Emerging roles for MAP kinases in agrin signaling. Commun. Integr. Biol. **4**:143–146.
4. **Jones NC, Fedorov Y V, Rosenthal RS, Olwin BB**. 2001. ERK1/2 is required for myoblast proliferation but is dispensable for muscle gene expression and cell fusion. J. Cell. Physiol. **186**:104–15.
5. **Yokoyama T, Takano K, Yoshida A, Katada F, Sun P, Takenawa T, Andoh T, Endo T**. 2007. DA-Raf1, a competent intrinsic dominant-negative antagonist of the Ras-ERK pathway, is required for myogenic differentiation. J Cell Biol, 2007/05/31 ed. **177**:781–793.
6. **Li J, Johnson SE**. 2006. ERK2 is required for efficient terminal differentiation of skeletal myoblasts. Biochem Biophys Res Commun, 2006/05/30 ed. **345**:1425–1433.
7. **Cho YY, Yao K, Bode AM, Bergen 3rd HR, Madden BJ, Oh SM, Ermakova S, Kang BS, Choi HS, Shim JH, Dong Z**. 2007. RSK2 mediates muscle cell differentiation through regulation of NFAT3. J Biol Chem, 2007/01/11 ed. **282**:8380–8392.
8. **Bennett AM, Tonks NK**. 1997. Regulation of Distinct Stages of Skeletal Muscle Differentiation by Mitogen-Activated Protein Kinases. Science (80-.). **278**:1288–1291.
9. **Shi H, Scheffler JM, Zeng C, Pleitner JM, Hannon KM, Grant AL, Gerrard DE**. 2009. Mitogen-activated protein kinase signaling is necessary for the maintenance of skeletal muscle mass. Am. J. Physiol. Cell Physiol. **296**:C1040–8.
10. **Shi H, Scheffler JM, Pleitner JM, Zeng C, Park S, Hannon KM, Grant AL, Gerrard DE**. 2008. Modulation of skeletal muscle fiber type by mitogen-activated protein kinase signaling. FASEB J, 2008/04/18 ed. **22**:2990–3000.
11. **Murgia M, Serrano AL, Calabria E, Pallafacchina G, Lomo T, Schiaffino S**. 2000. Ras is involved in nerve-activity-dependent regulation of muscle genes. Nat Cell Biol, 2000/03/09 ed. **2**:142–7.
12. **Roubenoff R, Hughes VA**. 2000. Sarcopenia: current concepts. J. Gerontol. A. Biol. Sci. Med. Sci. **55**:M716–24.
13. **Rahnert JA, Luo Q, Balog EM, Sokoloff AJ, Burkholder TJ**. 2011. Changes in growth-related kinases in head, neck and limb muscles with age. Exp. Gerontol. **46**:282–91.
14. **Muchir A, Kim YJ, Reilly SA, Wu W, Choi JC, Worman HJ**. 2013. Inhibition of extracellular signal-regulated kinase 1/2 signaling has beneficial effects on skeletal muscle in a mouse model of Emery-Dreifuss muscular dystrophy caused by lamin A/C gene mutation. Skelet. Muscle **3**:17.
15. **Tidyman WE, Rauen KA**. 2009. The RASopathies: developmental syndromes of Ras/MAPK pathway dysregulation. Curr. Opin. Genet. Dev. **19**:230–6.

16. **Tidyman WE, Lee HS, Rauen KA**. 2011. Skeletal muscle pathology in Costello and cardio-facio-cutaneous syndromes: developmental consequences of germline Ras/MAPK activation on myogenesis. Am. J. Med. Genet. C. Semin. Med. Genet. **157**:104–14.
17. **Stevenson DA, Allen S, Tidyman WE, Carey JC, Viskochil DH, Stevens A, Hanson H, Sheng X, Thompson BA, J. Okumura M, Reinker K, Johnson B, Rauen KA**. 2012. Peripheral muscle weakness in RASopathies. Muscle Nerve **46**:394–399.
18. **Rimer M**. 2010. Modulation of Agrin-induced Acetylcholine Receptor Clustering by Extracellular Signal-regulated Kinases 1 and 2 in Cultured Myotubes. J Biol Chem, 2010/08/11 ed. **285**:32370–32377.
19. **McMahan UJ**. 1990. The agrin hypothesis. Cold Spring Harb Symp Quant Biol **55**:407–418.
20. **Wu H, Xiong WC, Mei L**. 2010. To build a synapse: signaling pathways in neuromuscular junction assembly. Development, 2010/03/11 ed. **137**:1017–1033.
21. **Tansey MG, Chu GC, Merlie JP**. 1996. ARIA/HRG regulates AChR epsilon subunit gene expression at the neuromuscular synapse via activation of phosphatidylinositol 3-kinase and Ras/MAPK pathway. J Cell Biol **134**:465–476.
22. **Altiok N, Altiok S, Changeux JP**. 1997. Heregulin-stimulated acetylcholine receptor gene expression in muscle: requirement for MAP kinase and evidence for a parallel inhibitory pathway independent of electrical activity. EMBO J **16**:717–725.
23. **Si J, Mei L**. 1999. ERK MAP kinase activation is required for acetylcholine receptor inducing activity-induced increase in all five acetylcholine receptor subunit mRNAs as well as synapse-specific expression of acetylcholine receptor epsilon-transgene. Brain Res Mol Brain Res **67**:18–27.
24. **Ponomareva ON, Ma H, Vock VM, Ellerton EL, Moody SE, Dakour R, Chodosh LA, Rimer M**. 2006. Defective neuromuscular synaptogenesis in mice expressing constitutively active ErbB2 in skeletal muscle fibers. Mol Cell Neurosci **31**:334–345.
25. **Lutz CM, Kariya S, Patruni S, Osborne MA, Liu D, Henderson CE, Li DK, Pellizzoni L, Rojas J, Valenzuela DM, others**. 2011. Postsymptomatic restoration of SMN rescues the disease phenotype in a mouse model of severe spinal muscular atrophy. J Clin Invest **121**:3029–3041.
26. **Paez-Colasante X, Seaberg B, Martinez TL, Kong L, Sumner CJ, Rimer M**. 2013. Improvement of Neuromuscular Synaptic Phenotypes without Enhanced Survival and Motor Function in Severe Spinal Muscular Atrophy Mice Selectively Rescued in Motor Neurons. PLoS One **8**:e75866.
27. **Pagès G, Guerin S, Grall D, Bonino F, Smith A, Anjuere F, Auberger P, Pouyssegur J**. 1999. Defective Thymocyte Maturation in p44 MAP Kinase (Erk 1) Knockout Mice. Science (80-.). **286**:1374–1377.
28. **Selcher JC, Nekrasova T, Paylor R, Landreth GE, Sweatt JD**. 2001. Mice lacking the ERK1 isoform of MAP kinase are unimpaired in emotional learning. Learn Mem, 2001/02/13 ed. **8**:11–19.

29. **Hatano N, Mori Y, Oh-hora M, Kosugi A, Fujikawa T, Nakai N, Niwa H, Miyazaki J, Hamaoka T, Ogata M**. 2003. Essential role for ERK2 mitogen-activated protein kinase in placental development. Genes to Cells **8**:847–856.
30. **Saba-El-Leil MK, Vella FD, Vernay B, Voisin L, Chen L, Labrecque N, Ang SL, Meloche S**. 2003. An essential function of the mitogen-activated protein kinase Erk2 in mouse trophoblast development. EMBO Rep, 2003/09/23 ed. **4**:964–968.
31. **Yao Y, Li W, Wu J, Germann UA, Su MS, Kuida K, Boucher DM**. 2003. Extracellular signal-regulated kinase 2 is necessary for mesoderm differentiation. Proc Natl Acad Sci U S A, 2003/10/21 ed. **100**:12759–12764.
32. **Samuels IS, Karlo JC, Faruzzi AN, Pickering K, Herrup K, Sweatt JD, Saitta SC, Landreth GE**. 2008. Deletion of ERK2 mitogen-activated protein kinase identifies its key roles in cortical neurogenesis and cognitive function. J Neurosci, 2008/07/04 ed. **28**:6983–6995.
33. **Miniou P, Tiziano D, Frugier T, Roblot N, Le Meur M, Melki J**. 1999. Gene targeting restricted to mouse striated muscle lineage. Nucleic Acids Res. **27**:e27.
34. **Cifuentes-Diaz C, Frugier T, Tiziano FD, Lacene E, Roblot N, Joshi V, Moreau MH, Melki J**. 2001. Deletion of murine SMN exon 7 directed to skeletal muscle leads to severe muscular dystrophy. J Cell Biol, 2001/03/10 ed. **152**:1107–1114.
35. **Nicole S, Desforges B, Millet G, Lesbordes J, Cifuentes-Diaz C, Vertes D, Cao ML, De Backer F, Languille L, Roblot N, Joshi V, Gillis JM, Melki J**. 2003. Intact satellite cells lead to remarkable protection against Smn gene defect in differentiated skeletal muscle. J Cell Biol, 2003/05/14 ed. **161**:571–582.
36. **Escher P, Lacazette E, Courtet M, Blindenbacher a, Landmann L, Bezakova G, Lloyd KC, Mueller U, Brenner HR**. 2005. Synapses form in skeletal muscles lacking neuregulin receptors. Science **308**:1920–3.
37. **Balice-Gordon RJ**. 1997. Age-related chages in neuromuscular innervation. Muscle Nerve Suppl **5**:S83–S87.
38. **Li Y, Lee YI, Thompson WJ**. 2011. Changes in Aging Mouse Neuromuscular Junctions Are Explained by Degeneration and Regeneration of Muscle Fiber Segments at the Synapse. J Neurosci **31**:14910–14919.
39. **Valdez G, Tapia JC, Lichtman JW, Fox MA, Sanes JR**. 2012. Shared Resistance to Aging and ALS in Neuromuscular Junctions of Specific Muscles. PLoS One **7**:e34640.
40. **Valdez G, Tapia JC, Kang H, Clemenson GD, Gage FH, Lichtman JW, Sanes JR**. 2010. Attenuation of age-related changes in mouse neuromuscular synapses by caloric restriction and exercise. Proc Natl Acad Sci U S A **107**:14863–8.
41. **Lyons PR, Slater CR**. 1991. Structure and function of the neuromuscular junction in young adult mdx mice. J. Neurocytol. **20**:969–81.
42. **Rafael JA, Townsend ER, Squire SE, Potter AC, Chamberlain JS, Davies KE**. 2000. Dystrophin and utrophin influence fiber type composition and post-synaptic membrane structure. Hum. Mol. Genet. **9**:1357–67.
43. **Cheng A, Morsch M, Murata Y, Ghazanfari N, Reddel SW, Phillips WD**. 2013. Sequence of age-associated changes to the mouse neuromuscular junction and the protective effects of voluntary exercise. PLoS One **8**:e67970.

44. **Mauro A**. 1961. Satellite cell of skeletal muscle fibers. J. Biophys. Biochem. Cytol. **9**:493–5.
45. **Mishina M, Takai T, Imoto K, Noda M, Takahashi T, Numa S, Methfessel C, Sakmann B**. 1986. Molecular distinction between fetal and adult forms of muscle acetylcholine receptor. Nature **321**:406–411.
46. **Livak KJ, Schmittgen TD**. 2001. Analysis of relative gene expression data using real-time quantitative PCR and the 2(-Delta Delta C(T)) Method. Methods **25**:402–408.
47. **Gundersen K, Sanes JR, Merlie JP**. 1993. Neural regulation of muscle acetylcholine receptor epsilon- and alpha- subunit gene promoters in transgenic mice. J Cell Biol **123**:1535–1544.
48. **Son YJ, Thompson WJ**. 1995. Nerve sprouting in muscle is induced and guided by processes extended by Schwann cells. Neuron **14**:133–41.
49. **Witzemann V, Barg B, Nishikawa Y, Sakmann B, Numa S**. 1987. Differential regulation of muscle acetylcholine receptor gamma- and epsilon-subunit mRNAs. FEBS Lett. **223**:104–12.
50. **Wang X, Blagden C, Fan J, Nowak SJ, Taniuchi I, Littman DR, Burden SJ**. 2005. Runx1 prevents wasting, myofibrillar disorganization, and autophagy of skeletal muscle. Genes Dev. **19**:1715–22.
51. **Kues WA, Brenner HR, Sakmann B, Witzemann V**. 1995. Local neurotrophic repression of gene transcripts encoding fetal AChRs at rat neuromuscular synapses. J Cell Biol **130**:949–957.
52. **Schiaffino S, Reggiani C**. 2011. Fiber types in mammalian skeletal muscles. Physiol. Rev. **91**:1447–531.
53. **Guido AN, Campos GER, Neto HS, Marques MJ, Minatel E**. 2010. Fiber type composition of the sternomastoid and diaphragm muscles of dystrophin-deficient mdx mice. Anat. Rec. (Hoboken). **293**:1722–8.
54. **Bloemberg D, Quadrilatero J**. 2012. Rapid determination of myosin heavy chain expression in rat, mouse, and human skeletal muscle using multicolor immunofluorescence analysis. PLoS One **7**:e35273.
55. **Augusto V, Padovani CR, Eduardo G, Campos R**. 2004. SKELETAL MUSCLE FIBER TYPES IN C57BL6J MICE. Braz J Morphol Sci **21**:89–94.
56. **Flach RJR, Bennett AM**. 2010. MAP kinase phosphatase-1--a new player at the nexus between sarcopenia and metabolic disease. Aging (Albany. NY). **2**:170–6.
57. **Vantaggiato C, Formentini I, Bondanza A, Naldini L, Brambilla R**. 2006. Central ERK1 and ERK2 mitogen-activated protein kinases affect Ras-dependent cell signaling differentially. J Biol **5**:14.
58. **Shin S, Dimitri CA, Yoon S-O, Dowdle W, Blenis J**. 2010. ERK2 but not ERK1 induces epithelial-to-mesenchymal transformation via DEF motif-dependent signaling events. Mol. Cell **38**:114–27.
59. **Von Thun A, Birtwistle M, Kalna G, Grindlay J, Strachan D, Kolch W, von Kriegsheim A, Norman JC**. 2012. ERK2 drives tumour cell migration in three-dimensional microenvironments by suppressing expression of Rab17 and liprin-β2. J. Cell Sci. **125**:1465–77.
60. **Jang YC, Lustgarten MS, Liu Y, Muller FL, Bhattacharya A, Liang H, Salmon AB, Brooks S V, Larkin L, Hayworth CR, Richardson A, Van**

Remmen H. 2010. Increased superoxide in vivo accelerates age-associated muscle atrophy through mitochondrial dysfunction and neuromuscular junction degeneration. FASEB J. **24**:1376–90.

61. **Sakellariou GK, Davis CS, Shi Y, Ivannikov M V, Zhang Y, Vasilaki A, Macleod GT, Richardson A, Van Remmen H, Jackson MJ, McArdle A, Brooks S V**. 2014. Neuron-specific expression of CuZnSOD prevents the loss of muscle mass and function that occurs in homozygous CuZnSOD-knockout mice. FASEB J. **28**:1666–81.
62. **Zhang Y, Davis C, Sakellariou GK, Shi Y, Kayani AC, Pulliam D, Bhattacharya A, Richardson A, Jackson MJ, McArdle A, Brooks S V, Van Remmen H**. 2013. CuZnSOD gene deletion targeted to skeletal muscle leads to loss of contractile force but does not cause muscle atrophy in adult mice. FASEB J. **27**:3536–48.
63. **Banks GB, Chamberlain JS, Froehner SC**. 2009. Truncated dystrophins can influence neuromuscular synapse structure. Mol Cell Neurosci **40**:433–41.
64. **Merlie JP, Sanes JR**. 1985. Concentration of acetylcholine receptor mRNA in synaptic regions of adult muscle fibres. Nature **317**:66–68.
65. **Fontaine B, Sassoon D, Buckingham M, Changeux JP**. 1988. Detection of the nicotinic acetylcholine receptor alpha-subunit mRNA by in situ hybridization at neuromuscular junctions of 15-day-old chick striated muscles. EMBO J **7**:603–609.
66. **Simon AM, Hoppe P, Burden SJ**. 1992. Spatial restriction of AChR gene expression to subsynaptic nuclei. Development **114**:545–53.
67. **Brenner HR, Herczeg A, Slater CR**. 1992. Synapse-specific expression of acetylcholine receptor genes and their products at original synaptic sites in rat soleus muscle fibres regenerating in the absence of innervation. Development **116**:41–53.
68. **Barns M, Gondro C, Tellam RL, Radley-Crabb HG, Grounds MD, Shavlakadze T**. 2014. Molecular analyses provide insight into mechanisms underlying sarcopenia and myofibre denervation in old skeletal muscles of mice. Int. J. Biochem. Cell Biol. 1–12.
69. **Chai RJ, Vukovic J, Dunlop S, Grounds MD, Shavlakadze T**. 2011. Striking denervation of neuromuscular junctions without lumbar motoneuron loss in geriatric mouse muscle. PLoS One **6**:e28090.
70. **Pun S, Sigrist M, Santos AF, Ruegg MA, Sanes JR, Jessell TM, Arber S, Caroni P**. 2002. An intrinsic distinction in neuromuscular junction assembly and maintenance in different skeletal muscles. Neuron **34**:357–70.
71. **Punga AR, Lin S, Oliveri F, Meinen S, Rüegg MA**. 2011. Muscle-selective synaptic disassembly and reorganization in MuSK antibody positive MG mice. Exp. Neurol. **230**:207–17.
72. **Ling KKY, Gibbs RM, Feng Z, Ko C-P**. 2011. Severe neuromuscular denervation of clinically relevant muscles in a mouse model of spinal muscular atrophy. Hum Mol Genet **21**:185–195.
73. **Nowaczyk MJM, Thompson BA, Zeesman S, Moog U, Sanchez-Lara PA, Magoulas PL, Falk RE, Hoover-Fong JE, Batista DAS, Amudhavalli SM,**

White SM, Graham GE, Rauen KA. 2013. Deletion of MAP2K2/MEK2: a novel mechanism for a RASopathy? Clin. Genet. **85**:138–146.

855 **LEGENDS TO FIGURES**
856
857 **Figure 1. Mice generation and characterization of their ERK1/2 expression. (A)**
858 Sternomastoid (STN) and tibialis anterior (TA) extracts from 14-week-old mice were
859 probed simultaneously with antibodies to ERK2 and α-tubulin (α-Tub). Genotypes were:
860 Control: *Hsa-Cre*$^{-/-}$; *Erk2*$^{f/f}$. Het: *Hsa-Cre*$^{+/-}$; *Erk2*$^{f/+}$. *mErk2*^{CKO}: *Hsa-Cre*$^{+/-}$; *Erk2*$^{f/f}$.
861 Histograms show normalized quantification relative to control. A 90%-reduction in
862 ERK2 levels in both muscles in *mErk2*^{CKO} animals (n=3) relative to control (n=2) was
863 observed (**, $p<0.01$). **(B)** Same extracts in (A) were probed simultaneously with
864 antibodies to ERK1 and α-Tub. Histograms show normalized quantification relative to
865 control. A 20% reduction in ERK1 in *mErk2*^{CKO} muscle was observed (*, $p<0.05$). **(C)**
866 TA extracts from 14-week-old control, *Erk1*$^{-/-}$, *mErk2*^{CKO} and DKO mice were first
867 probed with antibodies to phosphorylated ERK1/2 (pERK1/2) (bottom panel). The blot
868 was stripped and reprobed simultaneously with antibodies to total ERK1/2 (tERK1/2) and
869 α-Tub (Top panel). ERK1 is totally absent in *Erk1*$^{-/-}$ and DKO muscle, and reduced
870 pERK2 in *mErk2*^{CKO} and DKO is in line with reduced tERK2 levels. Same results were
871 obtained with STN extracts (not shown). **(D)** Spinal cord (SPC), heart, kidney and liver
872 extracts from 9-week-old control and DKO mice probed with antibodies to tERK1/2 and
873 α-Tub. ERK2/α-Tub ratios are shown at the bottom of the blots. Except for kidney, no
874 reduction in ERK2 levels was observed in these tissues.
875 **Figure 2. DKO animals displayed stunted postnatal growth, muscle weakness and**
876 **shorter lifespan. (A)** Male weight progression was similar to control for *Erk1*$^{-/-}$ and
877 *mErk2*^{CKO} mice, whereas mild DKO animals failed to gain weight from around week 9
878 and severe DKO began losing weight around week 7. Similar weight progression was

seen in females (not shown). Per time-point: Control (n≥5); *Erk1*$^{-/-}$ (n≥6); *mErk2*^{CKO} (n≥7); mild DKO (n≥3, weeks 4-16; n=2, week 18); severe DKO (n≥4, weeks 4-10; n=2, week 11). DKO mild, p<0.01 vs. matching time-point control, t-test, starting at week 6 onwards. DKO severe, p<0.01 starting at week 5 onwards. **(B)** Forelimb grip strength was measured every other week starting at week 7 in males and females. Peak tension (g) was normalized to body weight (g). DKO mild and severe animals showed comparable decline in muscle strength, while *Erk1*$^{-/-}$ and *mErk2*^{CKO} mice were similar to control. Per time-point: Control (n≥4); *Erk1*$^{-/-}$ (n≥4); *mErk2*^{CKO} (n≥5); DKO mild (n≥4, weeks 7-13; n=2, week 15; n=1, week 17); DKO severe (n≥3, weeks 7-9; n=1, week 11). DKO mild and severe, p<0.01, ANOVA, week 9 onwards. **(C)** Mice were subjected to an accelerating rotarod protocol, and the time-to-fall (s) was recorded. No significant differences between controls and *Erk1*$^{-/-}$ or *mErk2*^{CKO} were resolved. DKO mild animals fell off the rotating drum consistently earlier than controls (p<0.01 vs. control, ANOVA). Per time-point: Control (n≥5); *Erk1*$^{-/-}$ (n≥3, week 9-17; n=2, week 19); *mErk2*^{CKO} (n≥5); DKO mild (n≥3, weeks 9-13; n=2, week 15; n=1, week 17). **(D)** Kaplan-Meier survival curves for DKO mild and severe mice. Median lifespan were: 71 days, n=23 (severe); 121 days, n=7 (mild); p<0.0001, Log-rank test. **(E)** A surviving female mild DKO mouse that developed kyphosis (arrowhead), absent in a matched control.

Figure 3. Fragmented NMJs in STN from young adult DKO mice. (A) An example of a control NMJ labeled with fluorescein-BTX to mark AChRs (A') and with antibodies to synaptophysin (SYN), followed by rhodamine-conjugated secondary antibodies, to label nerve terminals (A"). Long, continuous domains of postsynaptic AChRs are tightly apposed by nerve terminals. **(B)** and **(C)** Examples of fragmented NMJs in severe and

Molecular and Cellular Biology

mild DKO STN, respectively. Small, mostly round AChR domains variably apposed by nerve terminal staining. Scale bars: 10 µm.

Figure 4. Quantification of synaptic fragmentation in STN and TA. Number of AChR domains per endplate was counted from confocal maximal projections of NMJs in STN **(A)** and TA **(B)** from all 4 genotypes. Data were grouped in bins of 5 as represented in the X-axis, and the percent of NMJs in those bins were plotted in the Y-axis. STN: Control (n= 85 NMJs, 5 mice); *Erk1*$^{-/-}$ (80, 4); *mErk2*^{CKO} (90, 6); DKO (52, 3). TA: Control (n= 65, 4); *Erk1*$^{-/-}$ (32, 2); *mErk2*^{CKO} (112, 5); DKO (37,3). The results section describes the statistical analysis of the data.

Figure 5. Fragmented NMJs in *mErk2*^{CKO} STN and DKO TA. An example of a highly fragmented NMJ from *mErk2*^{CKO} STN **(A)**, a normal NMJ from control TA **(B)** and a fragmented NMJ from DKO TA muscle **(C)**. Overexposure in the rhodamine channel explains the strong intensity of the SYN staining in C''. Scale bars: 10 µm.

Figure 6. Quantification of central myonuclei in the STN. STN cross sections from 14-week-old mice were stained for H&E. 20X fields were selected, and total number of fibers and fibers with centrally located nuclei (arrows) were counted. Representative 20X field from control **(A)** and from mild DKO muscle **(B)**. Scale bar: 50 µm. **(C)** Quantification. Control, *Erk1*$^{-/-}$ and *mErk2*^{CKO} muscle had a similar proportion of fibers with central nuclei, while DKO had about twice as many. **, $p<0.01$ vs. control. N=3 muscles for all genotypes except *Erk1*$^{-/-}$ (n=2). Total fibers scored: Control, 1928; *Erk1*$^{-/-}$, 1234; *mErk2*^{CKO}, 1405; DKO, 1767.

Figure 7. Regulation of AChR expression by ERK1/2. (A) Examples of fields with DKO NMJs showing weaker (top panel) or faint (bottom panel) AChR staining (big

single arrowheads) relative to those in the same field that show more normal levels of AChR staining (small double arrowheads). Two examples of nerve terminal sprouts (arrows) in the DKO STN, labeled for SYN, are shown in the top panel. The short sprout in the bottom right appears to induce/connect with two small AChR clusters in the next myofiber. Scale bars: 10 µm. **(B)** Quantification of weak/faint BTX-stained NMJs. N= 2-6 muscles/genotype. **(C)** Real-time PCR for the adult AChR subunit mRNAs in 9-week-old STN and TA muscle. Values were normalized to control. A consistent decrease in *Chrne* mRNA was observed in *mErk2*^{CKO} and DKO muscle. **(D)** Real-time PCR for the fetal AChRγ subunit gene (*Chrng*) mRNA in 9-week-old STN and TA muscle. Values were normalized to control. A 40-fold increase in *Chrng* mRNA was detected selectively in DKO STN. (E) Real-time PCR for two additional denervation markers, *Runx-1* and *Myh3*. Values were normalized to control. Significant induction for these markers was restricted to DKO STN. For all real-time PCR assays, n=6 for both muscles and all genotypes except n=5 for *Erk1*$^{-/-}$ muscles. Muscles from both male and female animals were combined because no significant gender differences were found in the Ct values. *, $p<0.05$; **, $p<0.01$.

Figure 8. Reduced AChRε protein in DKO TA. AChRs were affinity purified from 1 mg-lysates from 3 control and 3 DKO TA muscles using biotin-BTX (BBTX) and streptavidin-agarose. Precipitates were subjected to SDS-PAGE, transferred to a PVDF membrane and probed for AChRε (arrow). Histogram shows average ± SEM of band intensities in arbitrary units. *, $p<0.05$.

Figure 9. Effects on fiber number, size and type. (A) Representative cross sections of STN muscles from 14-week-old female mice stained for dystrophin. Scale bar: 200 µm.

(B) Representative cross sections of TA muscles from 14-week-old female mice stained for dystrophin. Scale bar: 400 µm. **(C)** Quantification of fiber numbers. A significant reduction in total fibers per cross section was detected in the DKO STN. N=5 for controls and n=3 for all other genotypes. We combined data for males and females per genotype because no significant gender differences were found for this parameter. **(D)** Quantification of average fiber area. Because of gender differences in fiber area, raw data was normalized relative to control of the same sex. Controls were set at 100% and a one-sample t-test was used to statistically compare the results relative to control. N=3 for both muscles and all genotypes. DKO muscle had a smaller average fiber area that was statistically significant for the TA. **(E)** Distribution of fast fiber types in STN. Small but significant increases in 2X fibers were observed in muscles from *mErk2*^{CKO} and DKO mice. **(F)** Distribution of fast fiber types in TA. No changes in fiber type distribution due to genotype were observed in this muscle. We combined data within each muscle for males and females per genotype because no significant gender differences were found for this parameter. N=3 for both muscles and all genotypes. *, $p<0.05$; **, $p<0.01$.

Figure 10. Activated p38 in DKO muscle. (A) Control and DKO STN and TA extracts, n=3 per muscle/genotype, were probed with antibodies to phosphorylated p38 (pp38), total p38 (p38). Variations in loading were checked by stripping membranes and probing for α-Tub. **(B)** Normalized phosphorylated/total protein ratios for p38 showed no statistically significant changes in the activation of this kinase in DKO muscle relative to control.

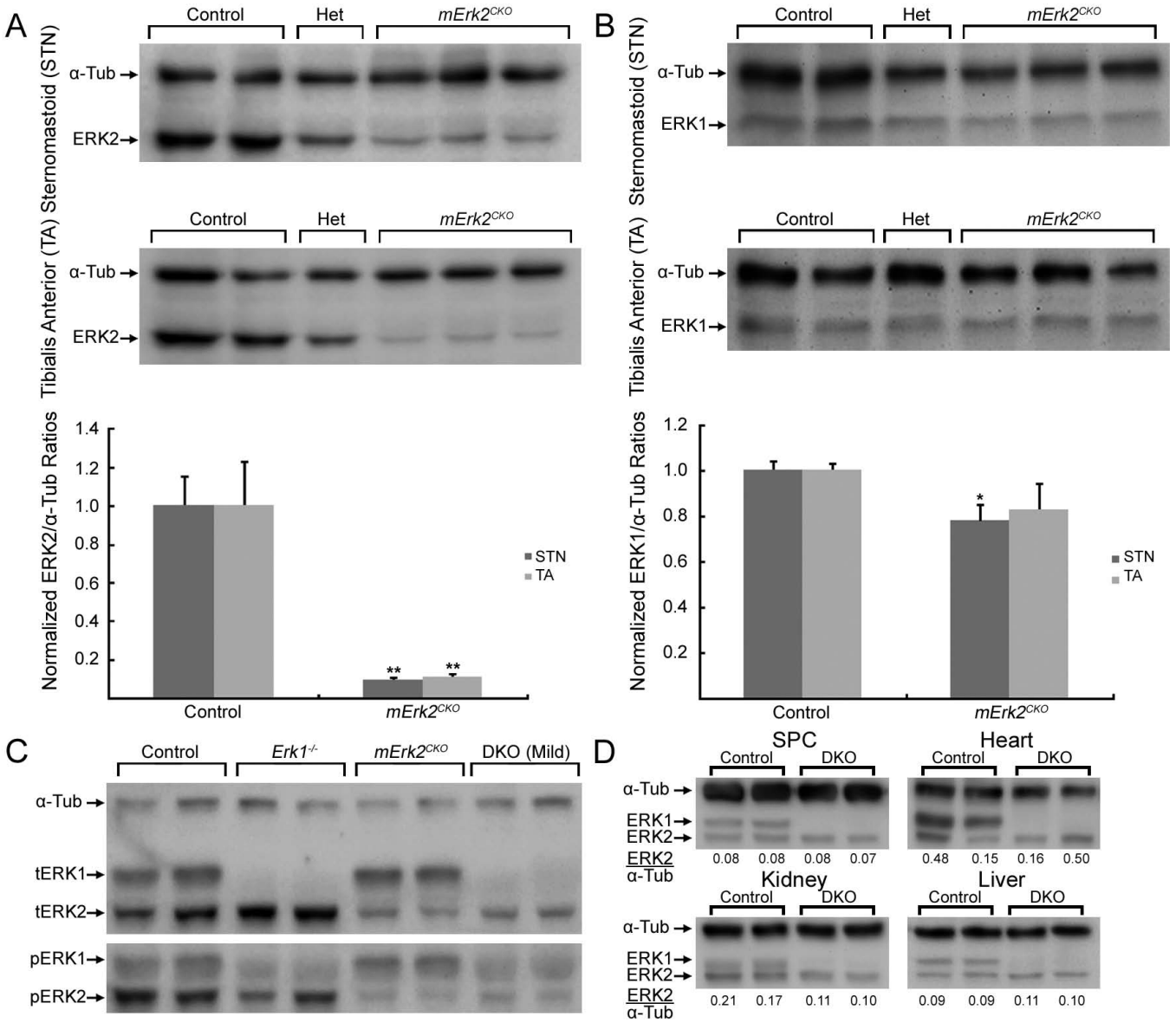

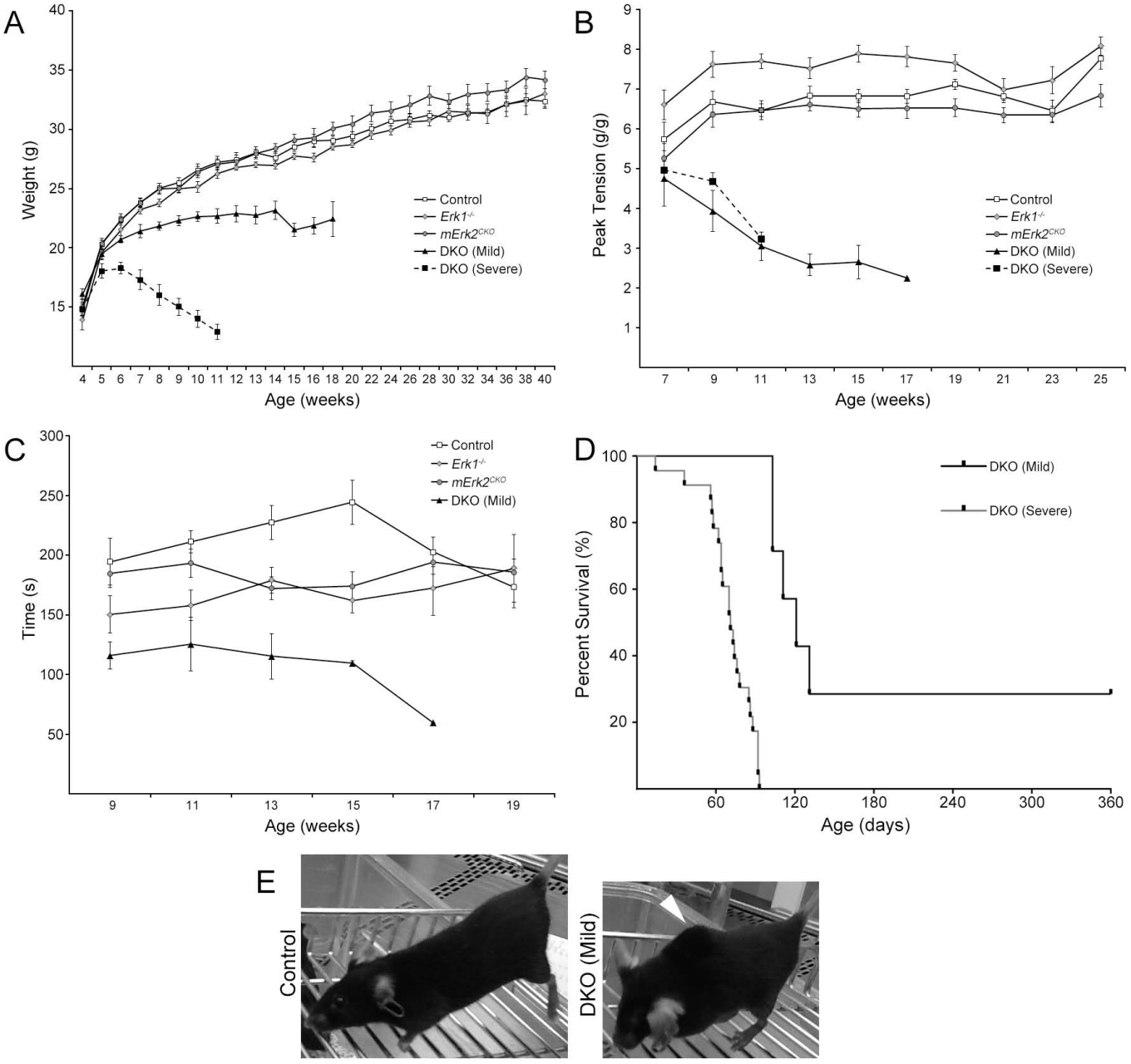

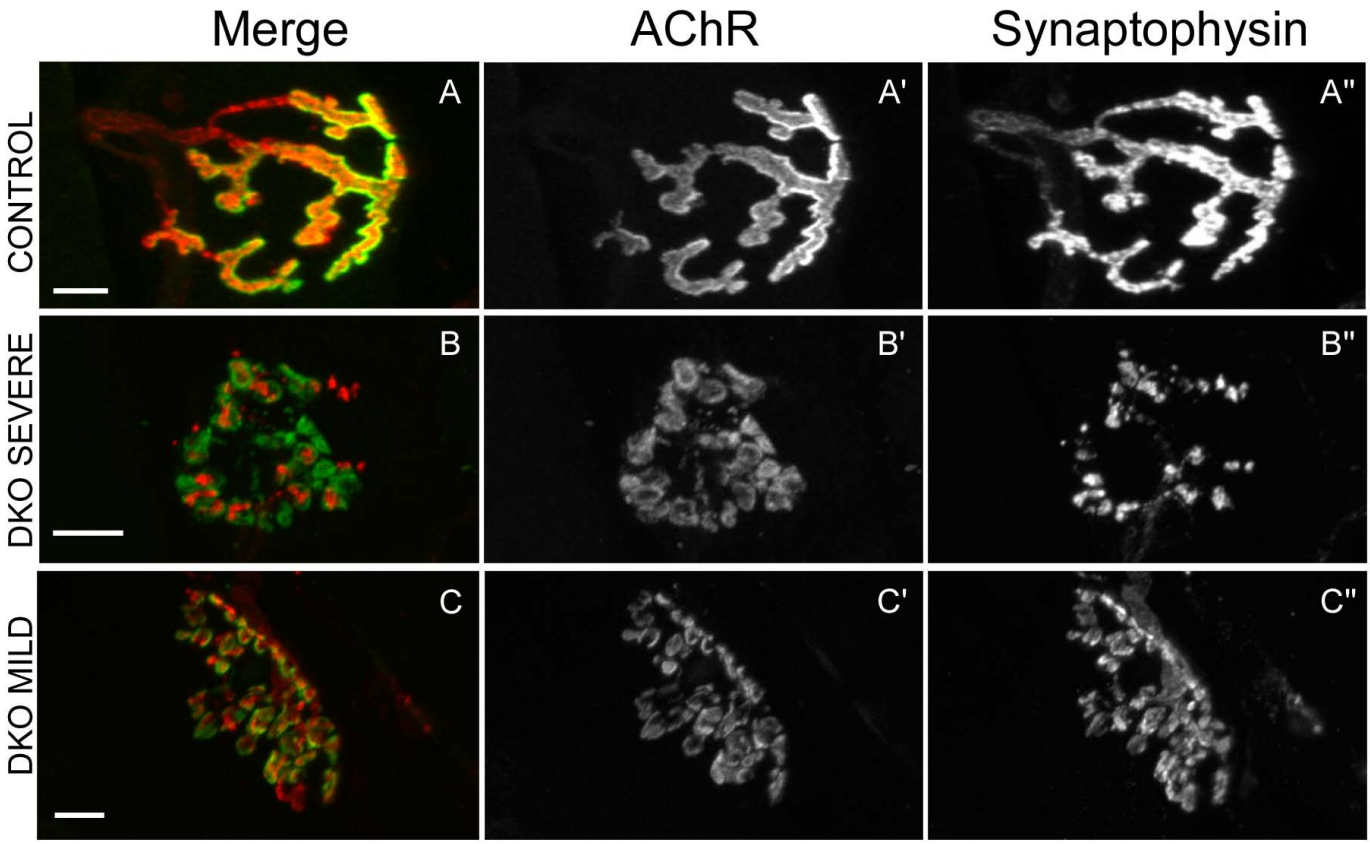

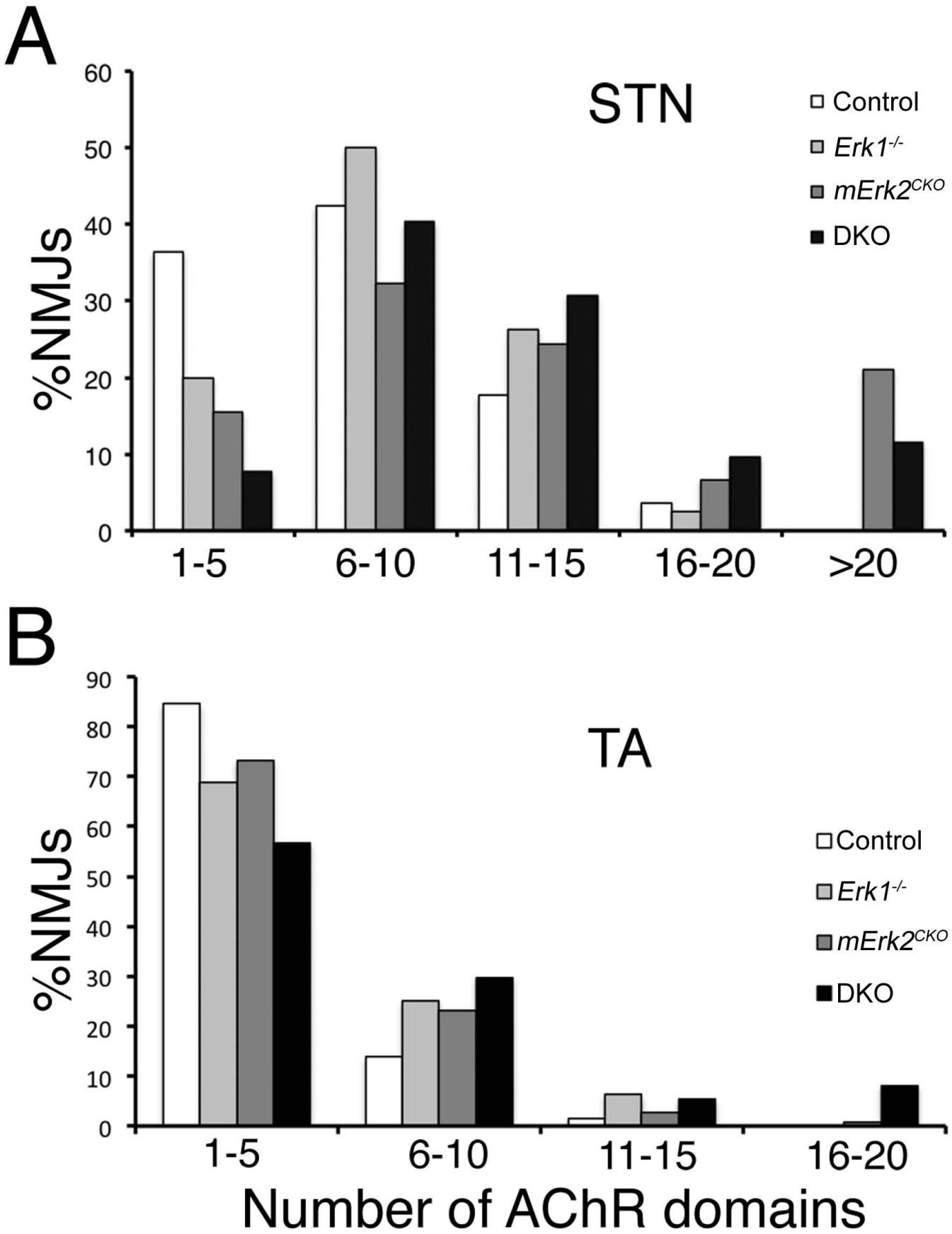

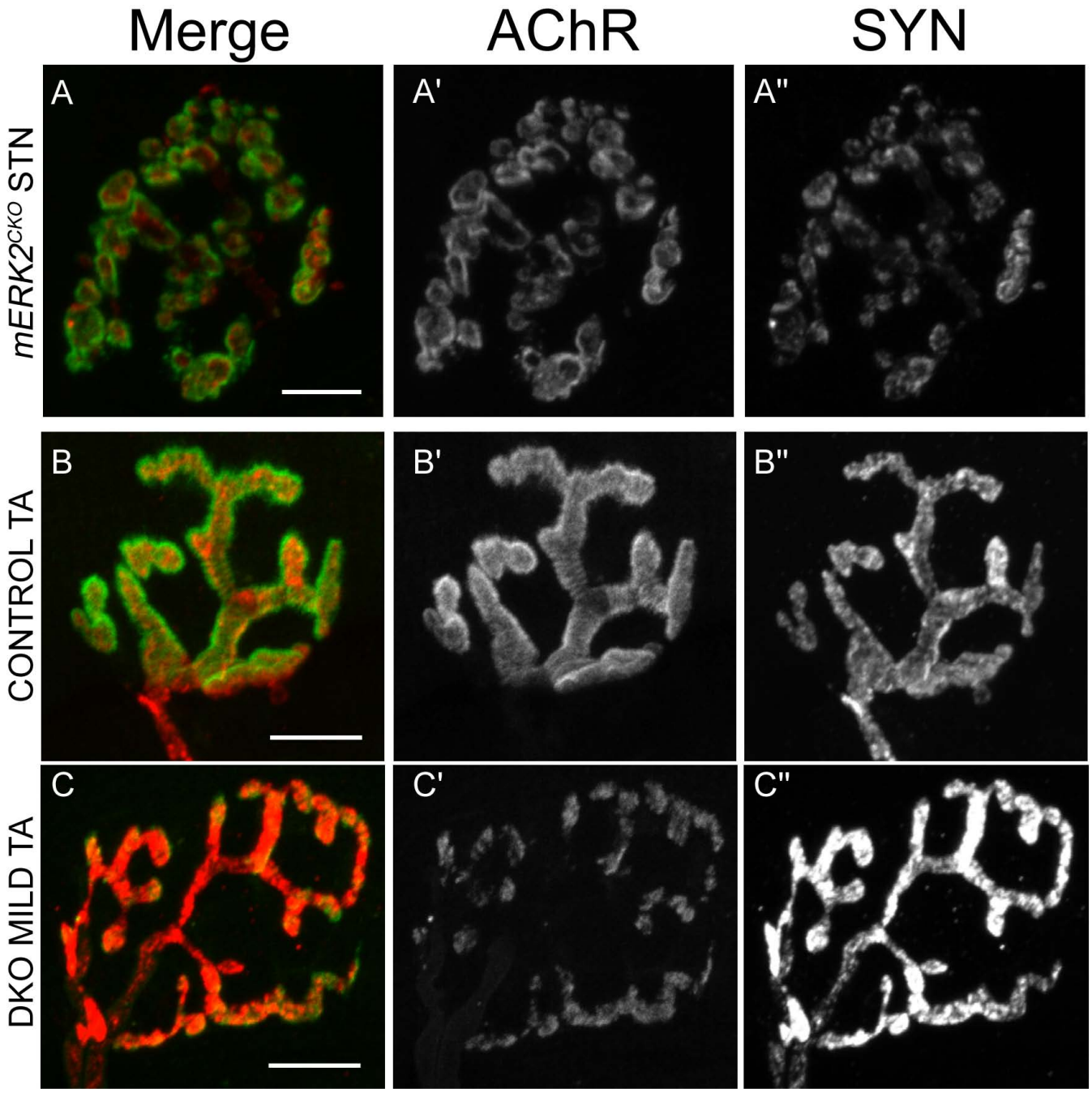

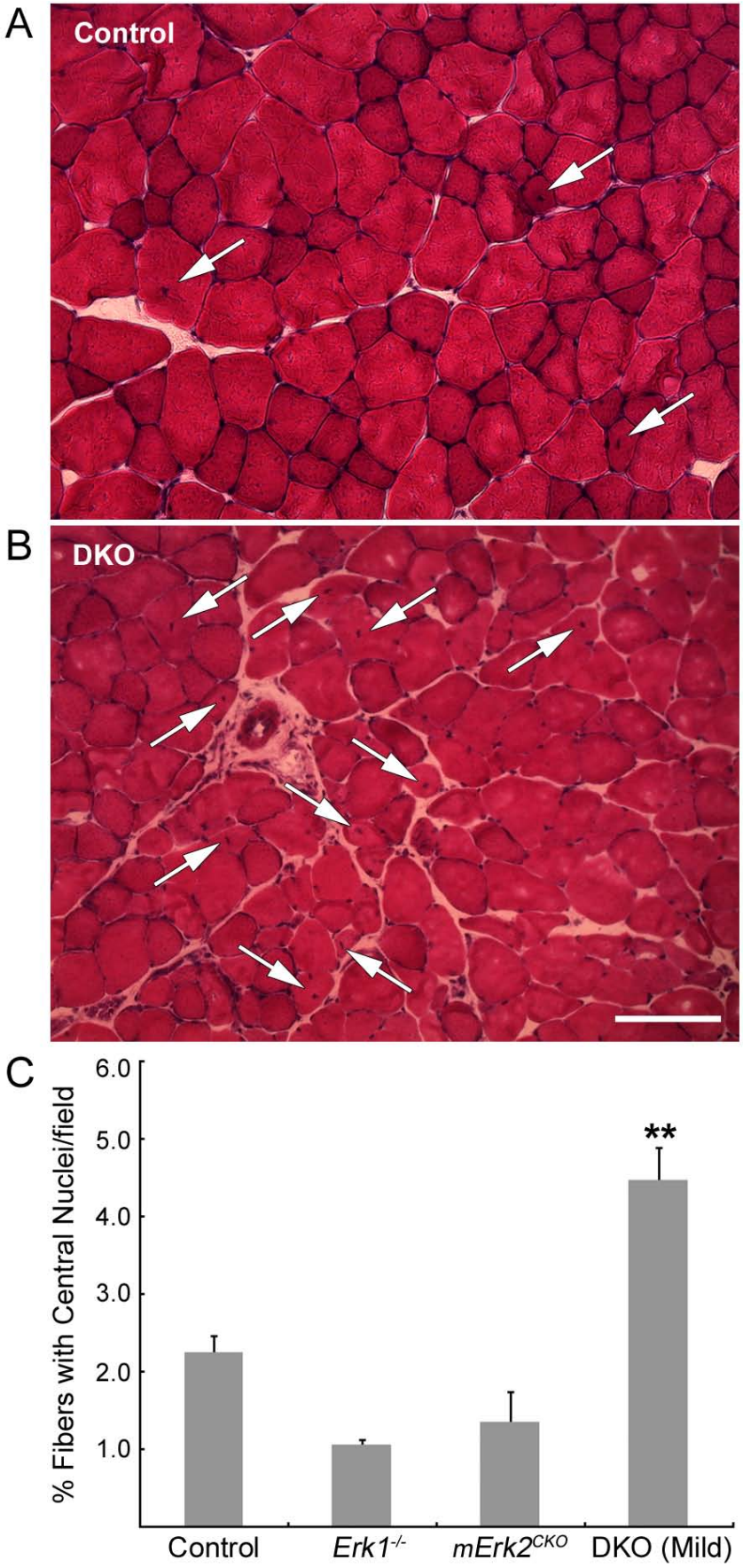

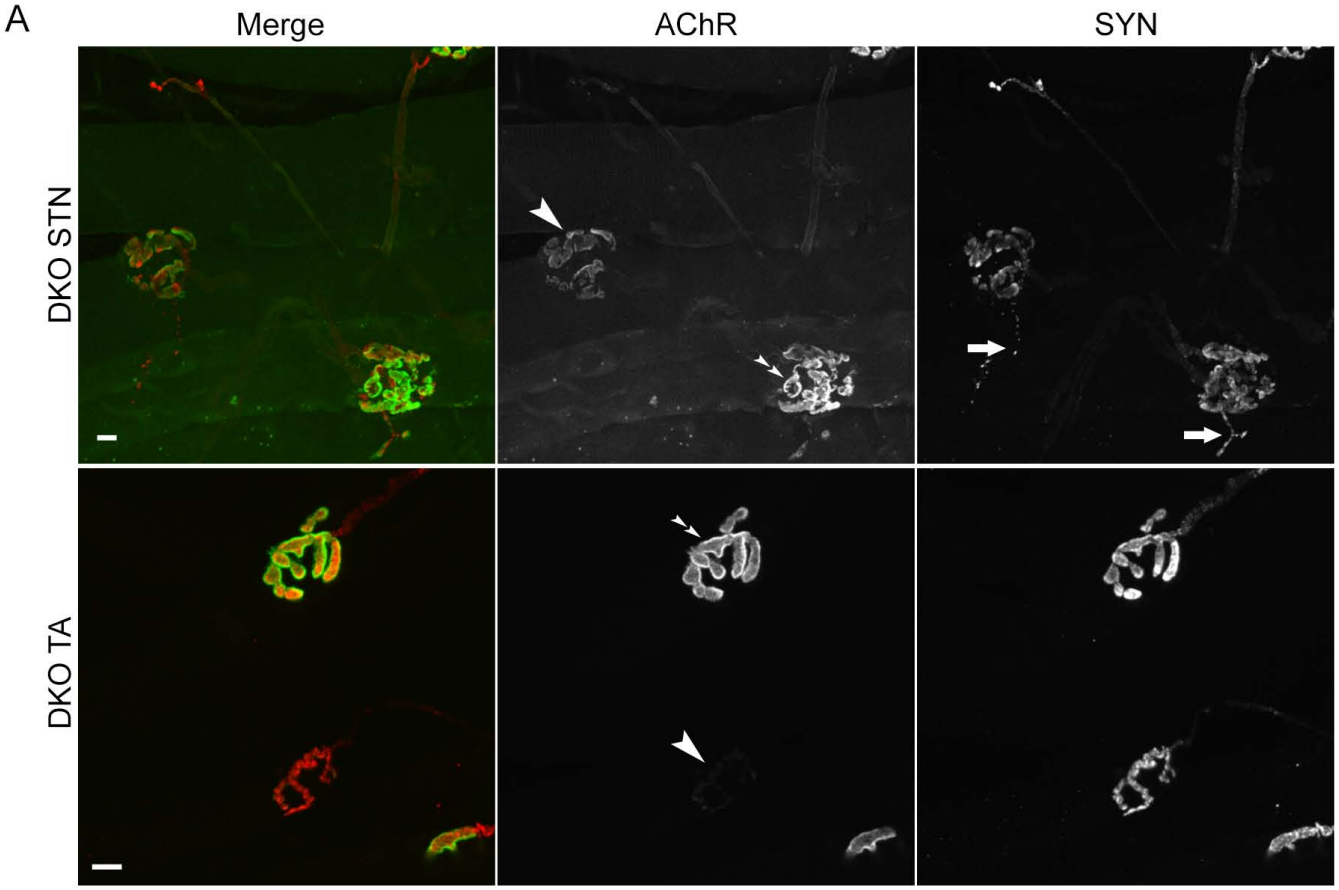

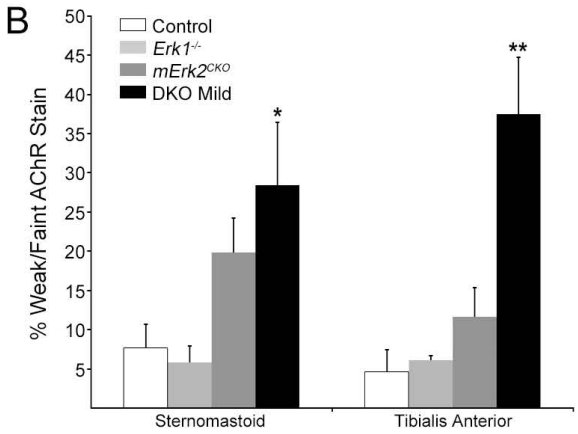

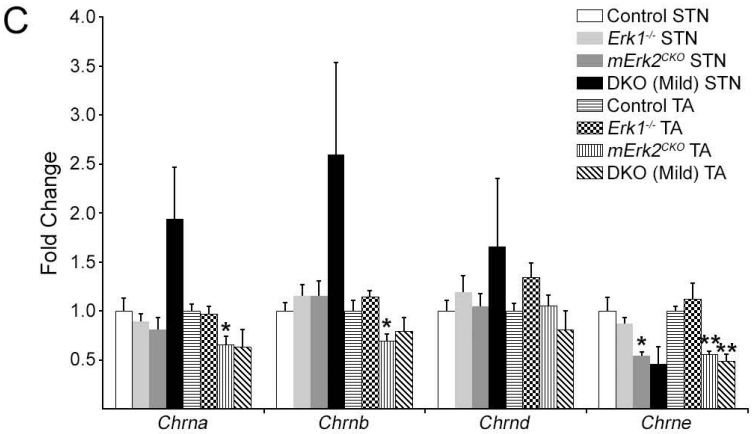

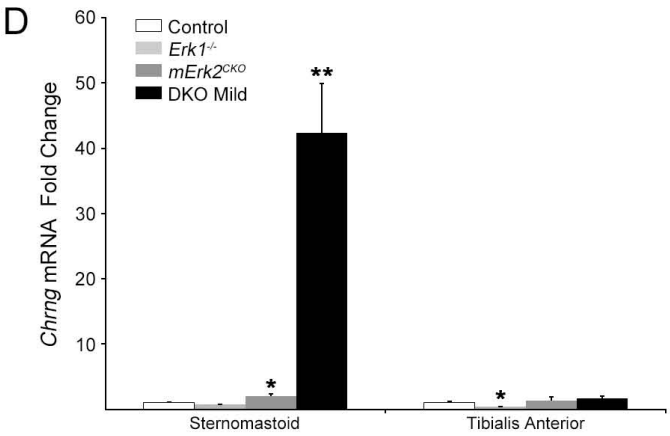

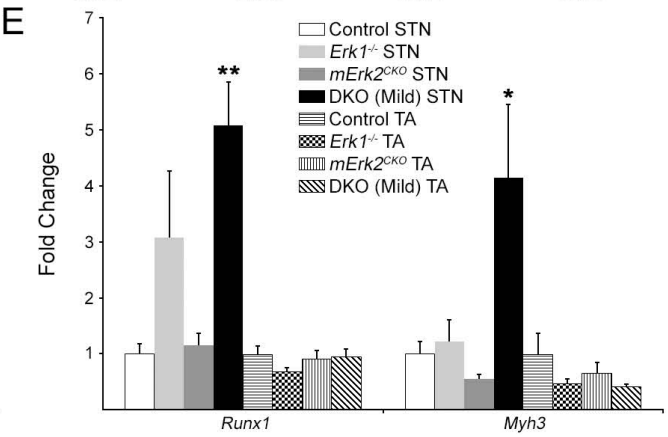

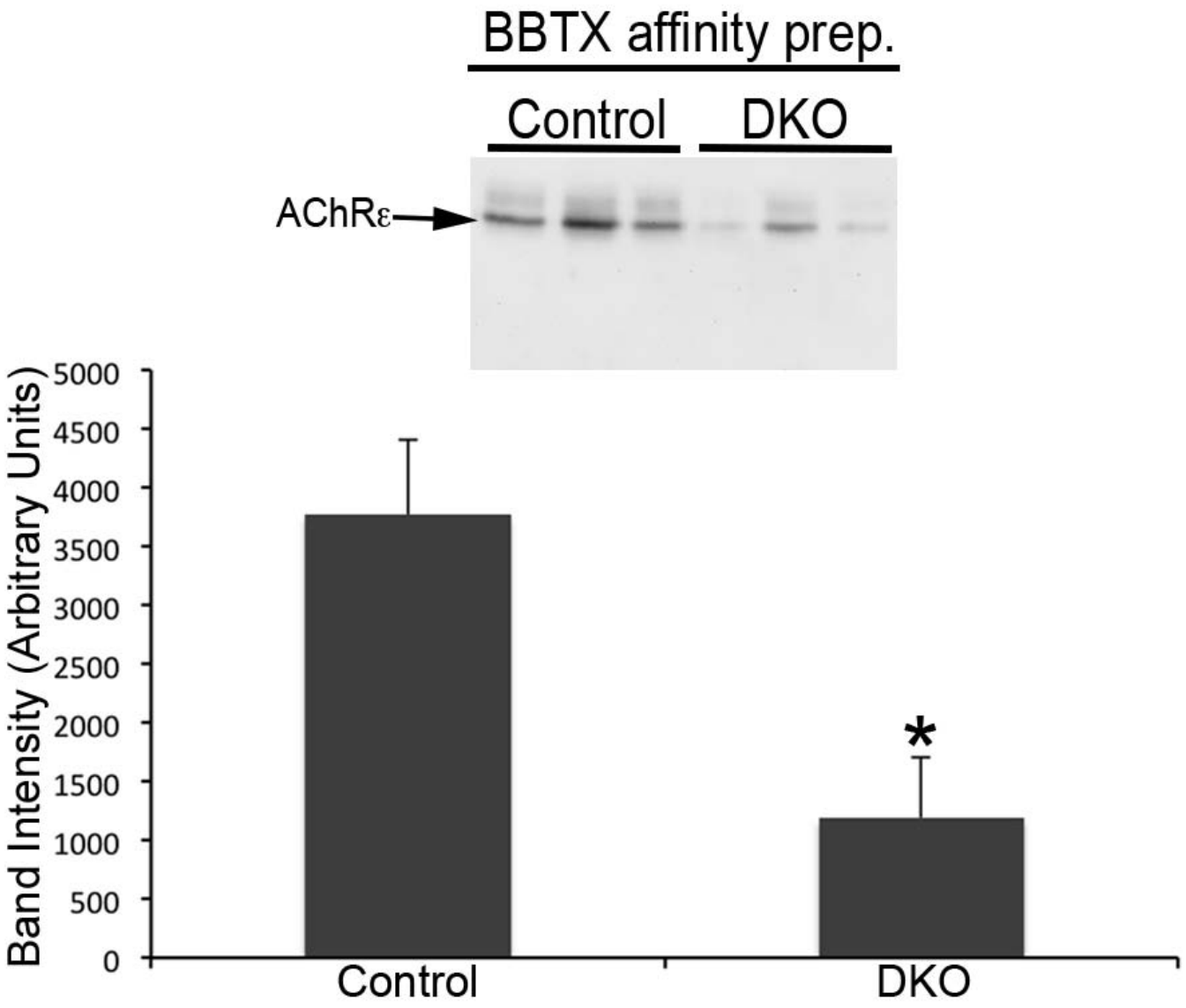

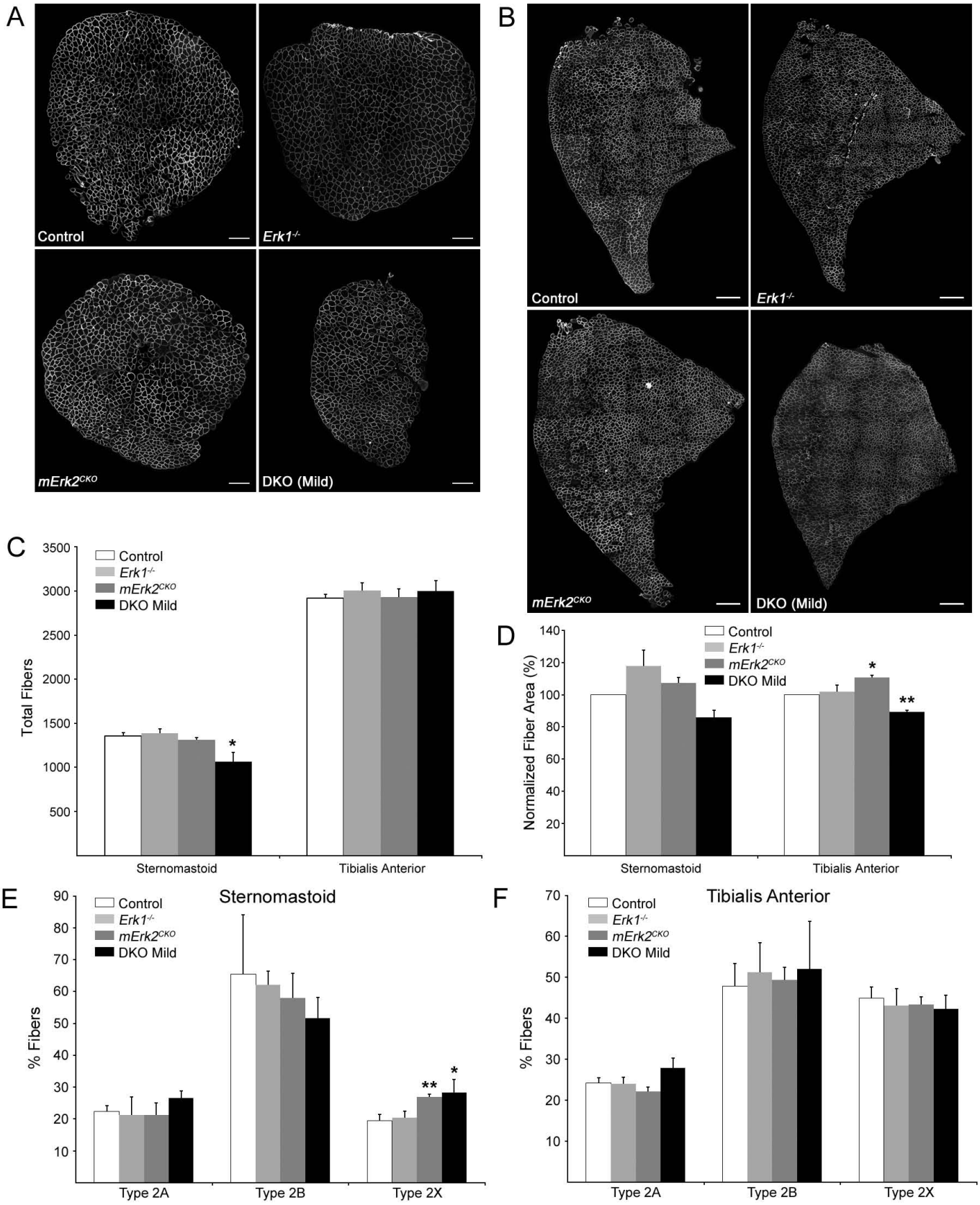

A

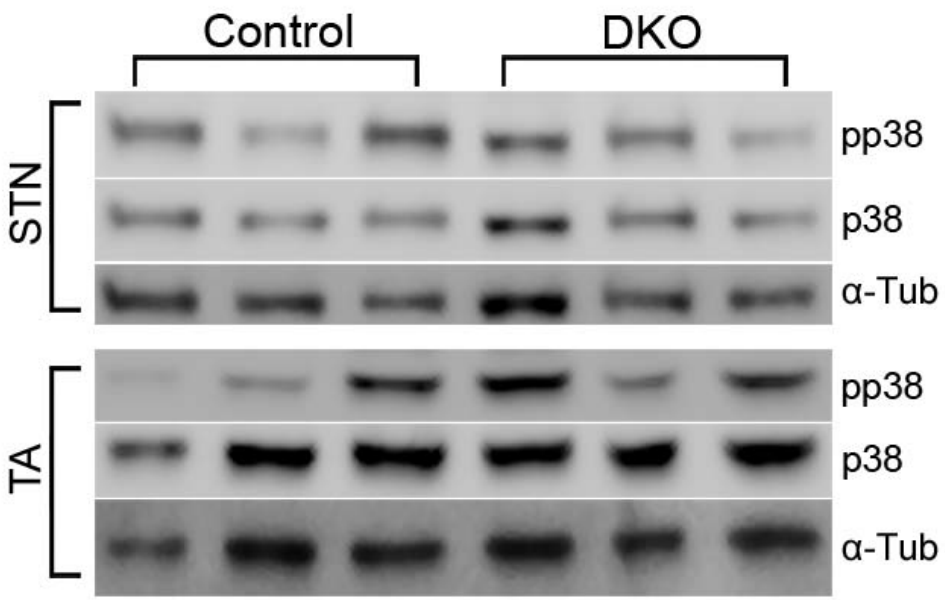

B